AD

Research and Development Technical Report
ECOM-0398-F

STUDY OF CYCLOTRON AND SYNCHRONOUS WAVE DEVICES

FINAL REPORT

BY

R. J. BRIGGS, S.F. PAIK

SEPTEMBER 1970

DDC
OCT 13 1970
RECEIVED
A

ECOM

UNITED STATES ARMY ELECTRONICS COMMAND · FORT MONMOUTH, N.J.
CONTRACT DAAB07-68-C-0398

MICROWAVE ASSOCIATES, INC.

Burlington, Massachusetts

AD 712323

NOTICES

Disclaimers

Disposition

Technical Report ECOM-0398-F

STUDY OF CYCLOTRON AND SYNCHRONOUS WAVE DEVICES

Final Report

1 July 1968 to 30 June 1970

Report No. 5

Contract No. DAAB07-68-C-0398

Prepared by

R. J. Briggs and S. F. Paik

Microwave Associates, Inc.
Burlington, Massachusetts

For

U. S. Army Electronics Command, Fort Monmouth, N. J. 07703

Distribution Statement

TABLE OF CONTENTS

ABSTRACT

It has been speculated for many years that microwave beam tubes using cyclotron and synchronous wave interactions could have a higher efficiency than is presently attainable in ordinary TWT's. This observation is based on the analysis of filamentary beam model which predicts that all electrons will lose an equal amount of axial energy when they interact with a circularly polarized traveling-wave circuit field. Under ideal conditions, therefore, the collector potential may be depressed close to the cathode potential; thus, very high efficiencies could be realized.

A theory of transverse-wave interactions with a more realistic model of the beam is developed to show that the main practical limitation arises from the fact that a moderate power electron beam must have a non-zero size and non-zero space charge density. The analysis of these effects leads to the following expression for the optimum efficiency with collector depression:

$$\text{Efficiency} = \left[\, 1 + (\text{beam diameter/r-f beam displacement}) \,\right]^{-1}$$

A nonlinear theory of the transverse-wave tubes is also developed to predict the saturation output power attainable. Unlike the large-signal theory of TWT's, it is possible to describe the non-linear behavior of transverse-wave tubes by a simple analytic expression. Numerical calculations of saturation characteristics are presented. The over-voltaged behavior of the tube under strong input drive is calculated to show that the power saturation due to velocity de-synchronization could be overcome by increasing the beam voltage.

Considering practical limitations of the beam parameters and the saturation characteristics, a set of possible design parameters of a high efficiency (> 50%), moderate power level (≈ 1 KW) transverse-wave

tube is obtained. The attainment of such goals with a reasonable circuit length appears difficult but is not excluded by our theory.

An experimental low-power vehicle operating in the 500-1000 MHz band was constructed to test the above theoretical predictions. Both the synchronous and the cyclotron wave interactions have been observed. The small-signal behavior as well as the saturation characteristics were in good agreement with the theory. Retarding potential measurements were made to determine the energy spread induced by the RF interactions. Experimental results, in general, tend to confirm the validity of the theoretical results.

LIST OF TABLES

I. INTRODUCTION

The original study of electron-beam waves with transverse RF modulation by Siegman[1] introduced many interesting concepts for new microwave devices. Most of the subsequent work in transverse-wave microwave tubes were motivated by expectations of either low-noise or high-efficiency devices. It has been shown both theoretically and experimentally that by selectively exciting the fast cyclotron wave (which carries positive energy) and removing the beam noise, one could obtain a class of low-noise parametric amplifiers.[2-8] It has also been pointed out, on the basis of the simple filamentary beam theory, that the interaction of a transverse beam wave with a circuit wave should not introduce a longitudinal velocity spread in the electron beam.[9,10] Based on this observation, it has been speculated that the efficiency of transverse-wave amplifiers with collector depression may be raised far beyond what is attainable in longitudinal-wave tubes. The present study of the transverse-wave devices was motivated by this promise of a class of high-efficiency microwave amplifiers.

As was pointed out by Siegman in his original paper,[1] the energy exchange mechanism in transverse-wave interactions does involve an extraction of energy from the longitudinal motion of the electrons. It is not immediately obvious, therefore, that one can automatically avoid a longitudinal velocity spread in a transverse-wave tube. Wessel-Berg[9] has shown theoretically how the coupler design can affect the axial velocity modulation. His basic conclusion, reasoning from the usual filamentary beam model, is that only one of the transverse modes should be excited to have a low velocity spread at the output of the coupler.

There have been only a limited number of experimental studies of the interaction between transverse beam waves and slow-wave circuits.

1

Johnson[11] has demonstrated interactions of both synchronous and cyclotron waves with a bifilar helix, and Hayes[12] has built a synchronous-wave amplifier in which a resonant interaction structure was used, as in a klystron. No attempt was made in either of these studies to investigate the velocity spread in the beam and the possible use of the interaction mechanism for a high-efficiency amplifier. The only experimental efforts aimed specifically at the achievement of high efficiencies in a transverse-wave tube were studies by Carroll[10] and Crumly and Larson.[13] Carroll's experiment on a cyclotron-wave traveling-wave tube were discouraging, as he was able to obtain an efficiency of only about 30% even with depressed collector operation. Experiments by Crumly and Larson were plagued by spurious oscillations and beam blow-up. No satisfactory theoretical explanation has been offered to account for the lack of success.

The interest in the high-efficiency amplifier is justified, if it can be shown that the high-efficiency predicted is attainable in a device with a relatively high power output. Theories of transverse-wave interactions, however, have not dealt with problems unique to high-power devices. The filamentary beam model most often used in the analytical study, for instance, is inadequate to describe a high-power beam, and the power saturation characteristics were unpredictable since there was no adequate nonlinear theory of transverse-wave interactions. In view of the unsuccessful experimental efforts and the lack of adequate theoretical foundations for design of high-power tubes, the emphasis in the present study has been on the theoretical understanding of the high-power behavior of transverse-wave tubes.

This report is divided into three major parts: First, in Section 2, we present a theory of transverse-wave interactions using a realistic model of the beam suitable for high-power amplifiers. The energy exchange mechanism in transverse-wave interactions is reviewed, and the energy

spread induced in a beam with non-zero size and space charge by high-power transverse-wave interactions is calculated. Various choices of design parameters are considered to show the basic design contraints in terms of the maximum efficiency attainable in high-power amplifiers. The power saturation characteristics of transverse-wave amplifiers are examined in Section 3 by analyzing the nonlinear behavior of transverse-wave interactions.

Results of the analyses in Sections 2 and 3 provide the theoretical basis for predicting capabilities and limitations of high-power, high-efficiency transverse-wave amplifiers. The purpose of the experimental study described in Section 4 was to verify the validity and determine limitations of various theoretical design equations. Experimental results presented in Section 4, by and large, confirm our theoretical predictions, and thus provide added credence to the theoretical projection of the potential device capabilities.

II. THEORY OF HIGH-POWER TRANSVERSE-WAVE TUBES

2.1 Introduction

The filamentary beam model often used in the analysis of transverse-wave tubes is inadequate to describe high-power tubes, since one must use a sizable beam with non-zero space charges in order to meet the beam-power requirements. In this section, we will analyze transverse-wave tubes with a realistic model of the beam to evaluate the effects the beam size and space charge. In Section 2.2, we will review the basic mechanism of energy exchange in traveling-wave type transverse-wave tubes to demonstrate in a clear physical way why a filamentary beam can lose axial energy without any spread being introduced. We then consider some of the practical limitations which constrain us from achieving these ideal conditions. In particular, we calculate in Section 2.3 the energy spread induced by transverse-wave interactions in an electron beam of finite diameter and finite space charges to show that the optimum efficiency (with collector depression) attainable in a transverse-wave tube is limited by these practical considerations. In Section 2.4, we consider in detail the possibility of designing high power, high efficiency transverse wave-amplifiers in view of the constrains derived in Section 2.3.

2.2 Filamentary Beam Theory of Transverse-Wave Amplifiers

Of the four transverse-beam waves originally introduced by Siegman, the slow cyclotron wave with positive polarization and the synchronous wave with negative polarization are the so-called negative-energy waves.[1] As in ordinary traveling-wave tubes, the coupling of negative-energy beam waves with waves propagating along a slow wave circuit leads to traveling-wave amplification. Therefore, there are two possible types of transverse-wave traveling-wave amplifiers: a synchronous wave tube and a cylotron wave tube. Figure 1 shows ω-β diagrams and

4
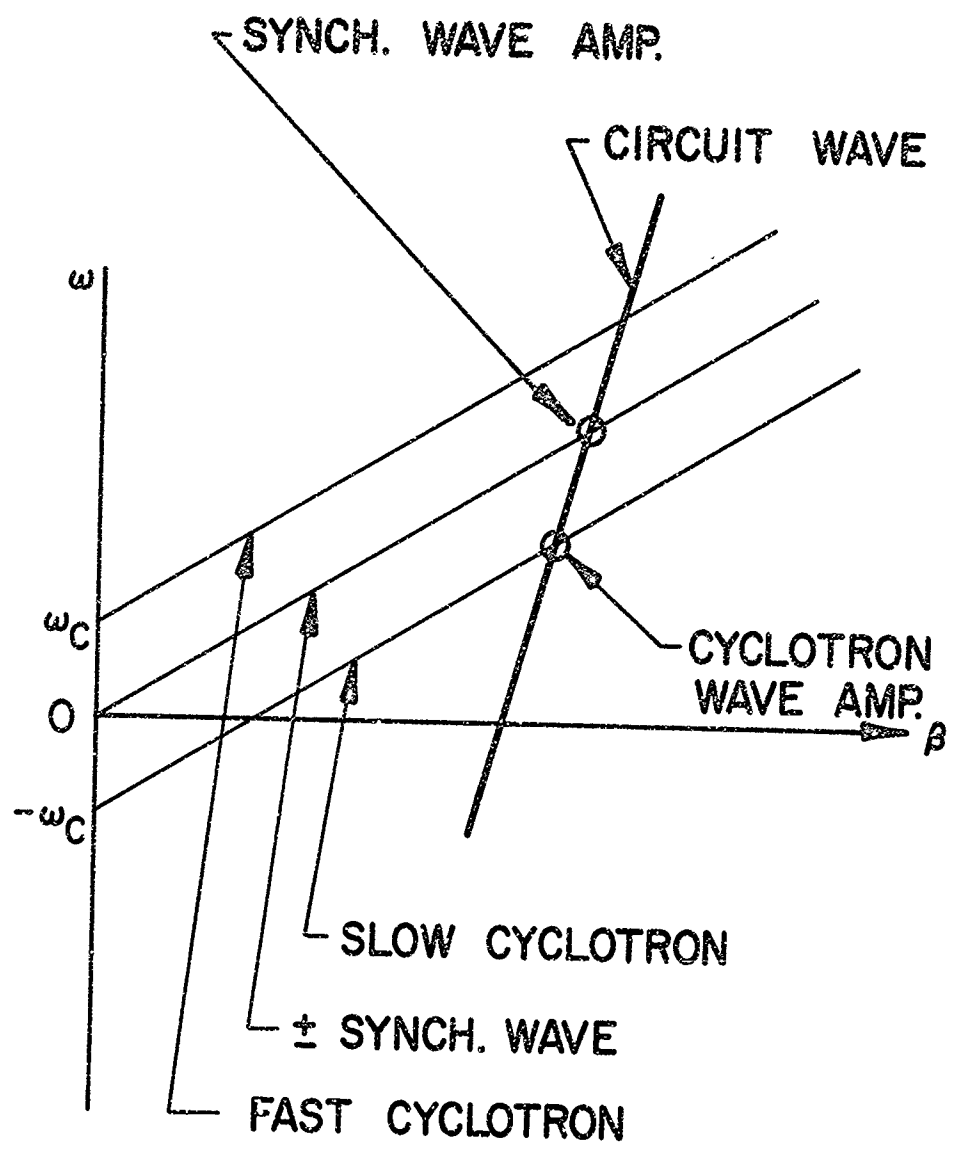
FIGURE 1 ω-β DIAGRAM FOR CYCLOTRON AND SYNCHRONOUS
WAVE AMPLIFIERS

5

the synchronism conditions required for the two types of traveling-wave amplifiers. Theoretical analyses of these amplifiers for gain, power output, bandwidth, etc., have been given by Siegman[1], Louisell[14] and others. Our analysis will follow that of previous authors, but our emphasis will be on the physical mechanism of energy transfer and the question of longitudinal velocity spread.

circuit field $(\bar{E}_c)$ that is purely transverse at the unperturbed beam position $(x = y = 0)$, and with a uniform axial magnetic field $\bar{B} = B_o \bar{i}_z$, is

$$\ddot{x} + \omega_c \dot{y} = -\eta E_{xc} \qquad (2.1)$$

$$\ddot{y} - \omega_c \dot{x} = -\eta E_{yc} \qquad (2.2)$$

In the above, $\dot{x}$ is the total-time derivative of x,

$$\dot{x} = \frac{dx}{dt} \approx \left(\frac{\partial}{\partial t} + v_o \frac{\partial}{\partial z} \right) x \qquad (2.3)$$

$\eta = e/m$, and $\omega_c = \eta B_o$ is the cyclotron frequency. For analytical convenience, we introduce the circularly polarized variables r and E_c where

$$r = x + jy \qquad (2.4)$$

$$E_c = E_{xc} + jE_{yc} \qquad (2.5)$$

The force equation can be written in terms of these variables as

$$\ddot{r} - j\omega_c \dot{r} = -\eta E_c \qquad (2.6)$$

To illustrate the meaning of the circularly polarized variables given in (2.4) and (2.5), note that a left polarized traveling-wave field is described by

$$E_c = E_o e^{j(\omega t - \beta z + \varphi)} \qquad (2.7)$$

with E_o real, since

$$E_{xc} = \frac{1}{2} (E_c + E_c{}^*) = E_o \cos (\omega t - \beta z + \varphi)$$

$$E_{yc} = \frac{1}{2j} (E_c - E_c{}^*) = E_o \sin (\omega t - \beta z + \varphi) \tag{2.8}$$

A right polarized wave, on the other hand, has $E_c \sim \exp \left[-j (\omega t - \beta z) \right]$.

2.2.1 Synchronous Wave

We now specialize to the synchronous wave interaction and assume (1) exact synchronism between the beam and the circuit wave,

$$\omega = \beta v_o \tag{2.9}$$

and (2) a purely circularly-polarized circuit field. Condition (2) can easily be achieved by an appropriate "twisted" type slow wave structure, and we should also note that a linearly polarized coupler would not result in a net energy exchange with the synchronous waves. We should also point out that throughout this work the circuit field "E_c" refers only to the space harmonic that is synchronous with the beam.

Under these assumptions, it is easily shown that the following is a solution of Eq. (2.6) and the boundary condition, $r(z = 0) = 0$

$$E_c = E_1 (e^{\alpha z} + e^{-\alpha z}) e^{j(\omega t - \beta z)} \tag{2.10}$$

$$r = a_1 (e^{\alpha z} - e^{-\alpha z}) e^{j(\omega t - \beta z)} \tag{2.11}$$

with

$$a_1 = \frac{n E_1}{j \alpha v_o \omega_c} \tag{2.12}$$

and where we have made the usual "low gain" assumption, $\alpha v_o \ll \omega_c$. An

7

expression for the gain constant α will be derived later in this section.

In the linear theory of transverse wave interactions, the longitudinal electric field at the beam does not usually appear explicitly, since it is a second-order quantity. All physical descriptions of the gain mechanism, however, show that it is this longitudinal field that is responsible for the energy conversion from the beam to the circuit wave. If the beam displacement from the axis is much less than a wavelength, then the longitudinal circuit field <u>at the beam position</u> is approximately

$$E_{zb} = \frac{\partial E_z}{\partial x} \, x + \frac{\partial E_z}{\partial y} \, y \qquad (2.13)$$

with (x, y) describing the beam position, since $E_z(0,0) = 0$. An electric field of a slow wave circuit with $\omega/\beta \ll c$ has $\nabla \times \vec{E} \approx 0$, and therefore

$$\frac{\partial E_z}{\partial x} \simeq \frac{\partial E_x}{\partial z}$$

$$\frac{\partial E_z}{\partial y} \simeq \frac{\partial E_y}{\partial z} \qquad (2.14)$$

The electric field at the beam can, therefore, be written as

$$E_{zb} = x \, \frac{\partial E_{xc}}{\partial z} + y \, \frac{\partial E_{yc}}{\partial z}$$

$$= \mathrm{Re}\left(r^* \frac{\partial E_c}{\partial z} \right) \qquad (2.15)$$

which for $\alpha \ll \beta$ is

$$E_{zb} \simeq \mathrm{Re} \, (-j\beta r^* E_c) \qquad (2.16)$$

8

Using Eqs. (2.10) and (2.11), the above becomes

$$E_{zb} = \frac{\eta \beta |E_1|^2}{\alpha v_0 \omega_c} (e^{2\alpha z} - e^{-2\alpha z})$$ (2.17)

The significance of Eq. (2.17) is that (outside of the slowly varying terms $e^{\pm 2\alpha z}$) the axial electric field seen by an electron is <u>constant</u> during its motion through the tube, and moreover, it is the <u>same</u> for all electrons, independent of their entrance phase with respect to the circuit field. If we integrate the axial equation of motion

$$\frac{dv_z}{dt} = -\eta E_{zb}$$ (2.18)

along the <u>unperturbed</u> electron trajectory, $z = v_0 (t - t_0)$, we have

$$v_z(z) - v_0 = \frac{-\eta^2 \beta |E_1|^2}{2\alpha^2 v_0^2 \omega_c} (e^{2\alpha z} + e^{-2\alpha z} - 2)$$

$$= - \frac{2\eta^2 \beta |E_1|^2}{\alpha^2 v_0^2 \omega_c} \sinh^2 \alpha z$$ (2.19)

with v_0 the injection velocity. According to this theory, a monoenergetic beam injected at $z = 0$ <u>remains</u> monoenergetic at the output, $z = \ell$. If we depress the collector to a potential that is above the cathode potential by an amount corresponding to the energy lost (to the circuit wave) by each and every electron, a theoretical electronic efficiency of 100% would be obtained.

The way in which the electrons give up energy to the circuit without developing any longitudinal modulation of their velocity is now physically clear. The electrons are initially located at $x = y = 0$ where there is no longitudinal electric field. The transverse electric field causes a radial displacement (essentially an $\bar{E} \times \bar{B}_0 / B_0^2$ motion) of the electrons

9

off axis into a region where there _is_ a longitudinal electric field. With a circularly polarized transverse electric field, all electrons arriving at a given position z are located the same distance from the axis, and (since $\omega = \beta v_o$) they also see a _constant_ phase of the longitudinal electric field during their transit through the tube.

As a check on the above explanation of the energy transfer mechanism, we will show how the application of energy conservation results in the well known expression for the gain constant, α. The time-average circuit power is given by

$$P_c(z) = \frac{|E_c(z)|^2}{2\beta^2 K_t} \tag{2.20}$$

in terms of the transverse interaction impedance, K_t. Energy conservation requires

$$\frac{\partial P_c}{\partial z} = P_B \tag{2.21}$$

where P_B is the net power lost by the electron beam (gained by the circuit) per unit length, and for synchronous waves

$$P_B = |I_o| E_{zb} \tag{2.22}$$

since the transverse energy acquired by the electrons is very small.

From Eqs. (2.17), (2.20), (2.21) and (2.22), we find that energy conservation is satisfied if

$$\alpha^2 = \beta^2 \frac{1}{2} \frac{I_o}{V_o} \frac{\omega}{\omega_c} K_t \tag{2.23}$$

where $V_o = v_o{}^2 / 2\eta$ is the beam voltage.

10

2.2.2 Cyclotron Wave

For synchronism with the slow cyclotron wave, we require a right polarized wave (or a reversed magnetic field, $\omega_c \rightarrow -\omega_c$). Except for this difference, we find that, with exact synchronism ($\omega - \beta v_o = -\omega_c$), the beam motion is given by Eqs. (2.11) and (2.12) with the +j replaced by (-j), and the longitudinal field at the beam is again given by Eq. (2.17). Therefore, all of the previous comments on the loss of axial kinetic energy without any spread being generated apply to cyclotron wave interactions as well. The main physical difference is that the transverse field "seen" by an electron in its rest frame is at the cyclotron frequency, and hence the perpendicular velocity is not small as it is with the synchronous wave. However, both the longitudinal electric field and the electrons "rotate around" the axis with the same pitch, so that the axial electric field seen by a particular electron remains constant (outside of the $e^{2\alpha z}$ frowth) during its transit.

With the cyclotron wave interaction, the transverse kinetic energy can be shown to be a factor of ω_c/ω times the magnitude of the change in the axial kinetic energy ($mv_o \Delta v_z$). In operating a depressed collector to achieve high efficiency with cyclotron waves, therefore, a scheme would have to be provided to convert this transverse energy back to longitudinal, such as the use of a diverging magnetic field at the collector. Otherwise the optimum theoretical efficiency would be limited to $(1 + \omega_c/\omega)^{-1}$.

2.3   Effects of Finite Beam Radius and Space Charge on the Energy Spread

It was shown in the previous section how the energy exchange mechanism with a filamentary beam involves motion of the beam electrons off axis into a region of finite longitudinal electric field. For a beam of

11

zero spot size, all of the electrons see the same longitudinal decelerating field, and hence the amplification of the circuit field proceeds by removing an identical amount of energy from each electron. This physical picture of the interaction mechanism immediately suggests that a finite size beam would not be monoenergetic at the output, since electrons initially at different radii would see different decelerating fields during their transit. The purpose of this section is to quantitatively assess this phenomenon.

The perturbed motion of the beam consists of a helical displacement in the transverse direction (Fig. 2) with the center of the beam located at $x_1(z,t)$, $y_1(z,t)$. We will ignore any distortions in the beam cross-section that arise from the pertubation; that is, we will assume at the outset that the beam retains its circular cross-section and has uniform charge density ρ_o. (Distortions in the cross-section will be small for a thin beam, and should have no substantial effect on the energy spread). Note also that we do not assume that the beam displacement is much less than the beam diameter in our treatment, so that the analysis is not "small signal" in the usual sense.

Our model is therefore fundamentally different from the models used in analyses of the effects of finite beam size and space charge on the dispersion characteristics of the transverse beam modes. We assume $\beta b \ll 1$, and for this case the uncoupled beam waves have dispersion characteristics that are closely approximated by the predictions of the filamentary beam model.[15, 16] On the other hand, the following analysis shows that the filamentary beam predictions regarding axial energy spread are only valid when the beam displacement greatly exceeds its diameter.

12
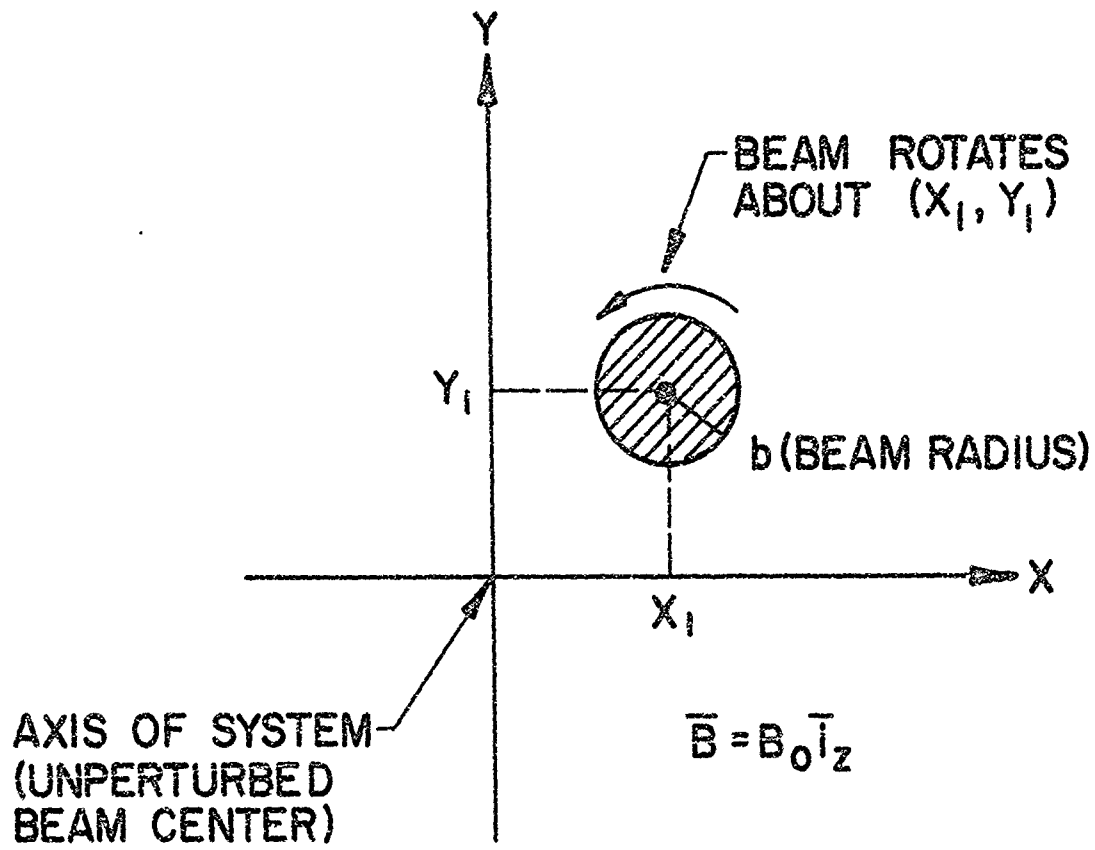
FIGURE 2   BEAM DISPLACEMENT VARIABLES

13

The electric field inside the beam is given by

$$E_x = \frac{\rho_o}{2\epsilon_o} (x - x_1) + E_{xc} \qquad (2.24)$$

$$E_y = \frac{\rho_o}{2\epsilon_o} (y - y_1) + E_{yc} \qquad (2.25)$$

where $\bar{E}_c$ is again the "circuit" electric field (the field arising from charges on the circuit structure), assumed constant in the regime of interest (a valid approximation if both the beam radius and the beam displacement are much less than $1/\beta$).

We again introduce the circularly polarized variables as in Eqs. (2.4) and (2.5) with $r(z,t)$ now describing the position of a <u>particular</u> electron in the beam cross-section. The force equation for the electrons is now

$$\ddot{r} - j\omega_c \dot{r} = \frac{\omega_p^2}{2} (r - r_1) - \eta E_c \qquad (2.26)$$

where $r_1 = x_1 + jy_1$ describes the beam center motion and $\omega_p = (-\eta \rho_o / \epsilon_o)^{1/2}$ is the plasma frequency.

2.3.1   Synchronous Wave Interaction

The circuit field is taken to be circularly polarized in the left hand sense, so that

$$E_c = E_1 e^{j(\omega t - \beta z)} \left[e^{\alpha z} + e^{-\alpha z} \right] \qquad (2.27)$$

14

We anticipate (and then prove) that the motion of the beam center has the form (c.f. Eqs. (2.10) and (2.11))

$$r_1 = a_1 e^{j(\omega t - \beta z)} \left[e^{\alpha z} - e^{-\alpha z} \right] \qquad (2.28)$$

In Eqs. (2.27) and (2.28) we have included both the growing and decaying parts of the solution. For simplicity, in the following analysis we will <u>explicitly exhibit only the growing wave part</u>, although the final answers will include both terms when we specialize to the case of perfect synchronism.

The solution of Eq. (2.26) for the transverse motion of a particular electron is (homogenous plus particular)

$$r(t,z) = r_0 e^{j\omega_R t} - \frac{\omega_R a_1 + nE_1/\omega_c}{\omega - \beta v_0 - \omega_R - j\alpha v_0} e^{j(\omega t - \beta z) + \alpha z} \qquad (2.29)$$

where

$$\omega_R = \frac{\omega_p^2}{2\omega_c} \qquad (2.30)$$

is the rotation frequency about the beam center and $r_0 = a_0 e^{j\phi_0}$ describes the position of the electron in the absence of a perturbation (basically a constant of integration). To obtain Eq. (2.29) we have made the following assumptions;

$$\omega_p^2 << \omega_c^2 \qquad (2.31)$$

$$\Omega \equiv \omega - \beta v_0 << \omega_c \qquad (2.32)$$

$$\alpha << \omega_c / v_0 \qquad (2.33)$$

15

with $v_z \simeq v_o$, the unperturbed axial velocity. Note also that in Eq. (2.29) the <u>unperturbed</u> motion of the electrons is assumed to be a simple rotation about the axis; that is, we have neglected the finite Larmor radius effects. As long as the magnetic field is at least a factor of two or more above the Brillouin value,[17] this is a sensible model of a physical beam. Such a "smooth" unscalloped beam could, in principle, be realized with the Brillouin magnetic field ($\omega_p = \omega_c/\sqrt{2}$ and $\omega_R = \omega_c/4$), but the achievement of this ideal in practice would be very difficult and, therefore, we will be conservative and assume inequality (2.31) in the following analysis.

To determine the displacement of the beam center, we note that by definition,

$$<r(t,z)> \equiv r_1(t,z) \tag{2.34}$$

where the brackets imply an average over φ_o. This yields

$$a_1 = \frac{\eta E_1/\omega_c}{j\alpha v_o - \Omega} \tag{2.35}$$

and the displacement of a particular electron is, therefore, given by

$$r(t,z) = r_o e^{j\omega_R t} + \frac{\eta E_1/\omega_c}{j\alpha v_o - \Omega} e^{j(\omega t - \beta z) + \alpha z}$$

$$= r_o e^{j\omega_R t} + a_1 e^{j(\omega t - \beta z) + \alpha z} \tag{2.36}$$

This result is intuitively clear; the net motion of an individual electron is simply the superposition of (1) the gyration at a frequency ω_R about the <u>instantaneous</u> beam center and (2) the common displacement of all electrons by an amount a_1 as given by Eq. (2.35). It is also interesting to note in Eq. (2.35) that the "pole" in a_1 is still at $\Omega = 0$, and is not shifted to $\Omega = \omega_R$ by the beam space charge.

16

To calculate the axial energy lost or gained by a particular electron, we need expressions for the axial component of the electric field. The axial component of the space-charge field (E_{zs}) can be determined by noting that for a thin beam the equipotentials associated with the space charge field inside the beam are approximately

$$\psi = - \frac{\rho_o}{4\epsilon_o} \left[(x - x_1)^2 + (y - y_1)^2 \right] \tag{2.37}$$

and, therefore,

$$
\begin{aligned}
E_{zs} &= - \frac{\partial \phi}{\partial z} \\
&= - \frac{\rho_o}{2\epsilon_o} \left[(x - x_1) \frac{\partial x_1}{\partial z} + (y - y_1) \frac{\partial y_1}{\partial z} \right] \\
&= - \frac{\rho_o}{2\epsilon_o} \, \text{Re} \left[(r - r_1) \cdot \frac{\partial r_1^*}{\partial z} \right]
\end{aligned}
\tag{2.38}
$$

From Eqs. (2.35), (2.36) and (2.38), we have

$$E_{zs} = - \frac{\omega_R}{\gamma v_o} \, a_o E_1 \cos \left[\omega t - \beta z - \omega_R t - \phi_o \right] (e^{\alpha z} - e^{-\alpha z}) \tag{2.39}$$

as the longitudinal space-charge field seen by the electron _at synchronism_ $(\omega \equiv \beta v_o)$. Note also that we have now included the decaying part of the solution as well as the growing part in Eq. (2.39).

The longitudinal circuit field at the beam position is again given by Eq. (2.15), and from Eq. (2.36) and (2.27) we find

17

$$E_{zc} = \frac{\eta E_1^2 \beta}{\alpha v_o \omega_c} (e^{2\alpha z} - e^{-2\alpha z}) +$$

$$\beta a_o E_1 (e^{\alpha z} + e^{-\alpha z}) \sin (\omega t - \beta z - \omega_R t - \phi_o) \qquad (2.40)$$

In addition to the second order longitudinal circuit field common to all electrons (first term in (2.40)), there is now a first order longitudinal circuit field at the electron's position that depends on the initial location of the electron within the beam cross-section.

The longitudinal force equation is

$$\frac{dv_z}{dt} = -\eta (E_{zs} + E_{zc}) \qquad (2.41)$$

which integrates along the underlined unperturbed electron trajectory to yield

$$v_z - v_o = -\frac{\eta^2 E_1^2 \beta}{2\alpha^2 \cdot v_o^2 \omega_c} (e^{2\alpha z} + e^{-2\alpha z} - 2)$$

$$-\frac{\eta \beta a_o E_1}{\alpha v_o} \sin (\omega t - \beta z - \omega_R t - \phi_o) (e^{\alpha z} - e^{-\alpha z}) \qquad (2.42)$$

(This expression for Δv_z as a function of z and t is, of course, invalid whenever Δv_z gets large enough so that the electrons begin to drop out of synchronism with the circuit wave; i.e., when $|\omega - \beta v_z|$ becomes comparable to αv_o).

Keeping terms up to second order, we now have the following expression for the kinetic energy in electron volts of the electron described by the initial position a_o, φ_o. (Note that the transverse velocity is

18

negligible for a synchronous wave).

$$W_k = \frac{v_z^2}{2\eta}$$

$$\approx \frac{v_o^2}{2\eta} - \frac{nE_1^2 \omega'}{2\alpha^2 v_o^2 \omega_c} (e^{\alpha z} - e^{-\alpha z})^2 + \frac{nE_1^2 (\beta \alpha_o)^2}{2\alpha^2 v_o^2} (a^{\alpha z} - e^{-\alpha z})^2 \sin^2(\omega t - \beta z - \omega_R t - \phi_c)$$

$$- \frac{E_1}{\alpha} (\beta a_o) (e^{\alpha z} - e^{-\alpha z}) \sin(\omega t - \beta z - \omega_R t - \phi_o) \qquad (2.43)$$

Note that the last term in Eq. (2.43) is first order in E_1, and that it changes sign over the beam cross-section. That is, at a given instant of time and given position z, electrons in a particular sector of the beam have lost more than the average energy while those in the opposite sector have lost less than the average (Fig. 3). (In this discussion we ignore the third term in Eq. (2.43) since it is of higher order). As time goes on, these sectors of the beam "rotate" around. On the other hand, if we ask for the average kinetic energy lost by all the electrons in a particular cross-section of the beam, this last term will drop out, and we get the following for the average energy lost.

$$\triangle \epsilon_L = -\int_o^b \int_o^{2\pi} W_k \frac{d\phi_o a_o da_o}{\pi b^2} + \frac{v_o^2}{2\eta}$$

$$= \frac{nE_1^2 \omega}{2\alpha^2 v_o^2 \omega_c} \left(1 - \frac{1}{4} \frac{\omega_c}{\omega} \beta^2 b^2 \right) (e^{\alpha z} - e^{-\alpha z})^2 \qquad (2.44)$$

19
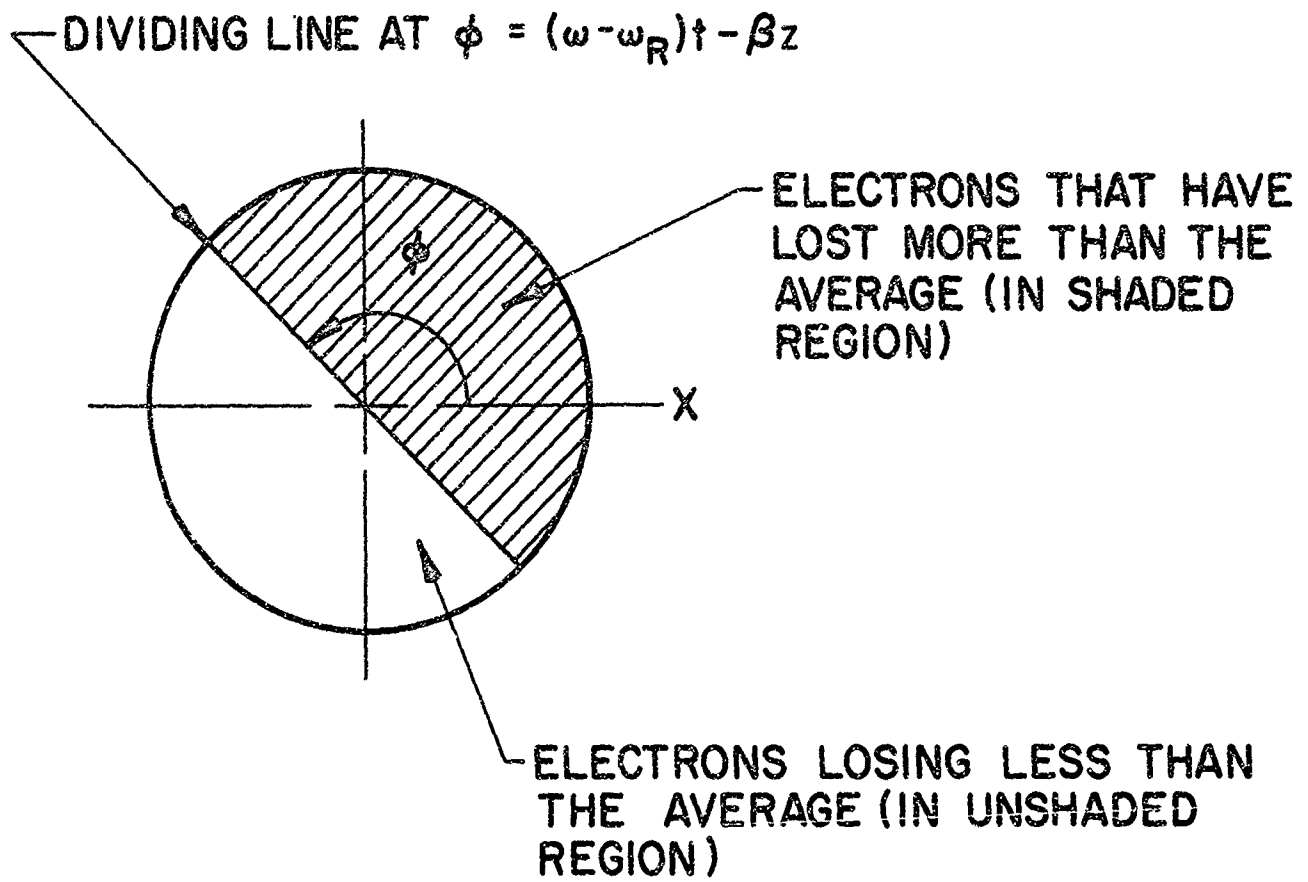
FIGURE 3   ILLUSTRATION OF THE ENERGY DISTRIBUTION OF
ELECTRONS OVER THE BEAM CROSS SECTION

20

Note that we must have

$$\frac{1}{4} \frac{\omega_c}{\omega} (\beta b)^2 < 1 \tag{2.45}$$

to have any net loss of energy by the electrons. We will assume in the following that this finite-radius correction term is very small, since the validity of our model requires $\beta b \ll 1$.

The mean energy loss of all electrons, of course, is the only relevant quantity when computing the small signal gain and the power output. (c.f., Eq. 2.46). In considering the enhancement of amplifier efficiency by collector depression, however, the distribution of electron energies is also of importance. From Eq. (2.43), it is clear that the energy loss of any particular electron can differ from the mean loss $(\Delta\epsilon_L)$ by as much as $\pm \Delta\epsilon_s$, with

$$\epsilon_s = \frac{E_1}{\alpha} \beta b (e^{\alpha z} - e^{-\alpha z}) \tag{2.46}$$

The energy distribution of the electrons at the output would, therefore, look roughly as shown in Fig. 4. The significance of $\Delta\epsilon_s$ is as follows. A (properly designed) collector could be depressed to a voltage of

$$V_{coll} = - (V_o - \Delta\epsilon_L - \Delta\epsilon_s) \tag{2.47}$$

without returning any electrons. $(-V_o)$ is cathode voltage with respect to circuit. The (net) dc power supplied to the beam is then

$$P_{dc} = I_O (\Delta\epsilon_L + \Delta\epsilon_s) \tag{2.48}$$

21

NO. OF
ELECTRONS
PER SEC.

$2\Delta\epsilon_s$

$\Delta\epsilon_L$

ENERGY IN eV

V_0

(INJECTION VOLTAGE)
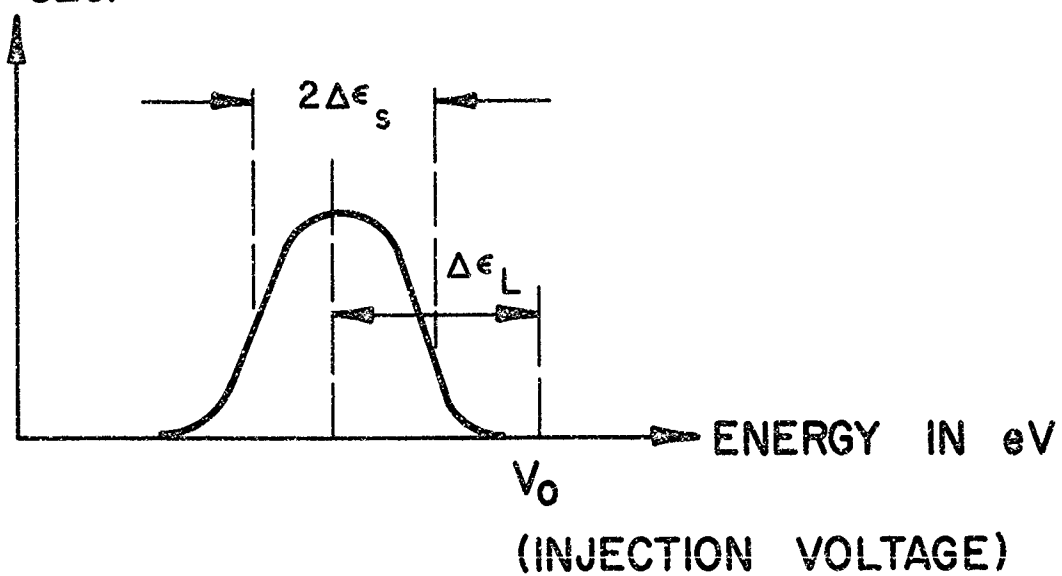
FIGURE 4   ELECTRON ENERGY DISTRIBUTION AT THE OUTPUT
OF THE RF INTERACTION REGION

22

On the other hand, the increase in the RF power output is equal to the average energy lost by the electrons, as was shown in Section 2.2. That is,

$$P_{out} - P_{in} = P_{e\ell} = I_o \Delta \varepsilon_L \tag{2.49}$$

Therefore, the maximum efficiency with collector depression is

$$\eta_{opt} = \frac{P_{e\ell}}{P_{dc}} = \frac{1}{1 + \Delta \varepsilon_s / \Delta \varepsilon_L} \tag{2.50}$$

(The validity of this formula is clearly restricted to the domain $\Delta \varepsilon_s + \Delta \varepsilon_L < V_o$; the implications of this restriction are discussed in more detail in the following section).

For the highest possible theoretical efficiency, we should keep $\Delta \varepsilon_s / \Delta \varepsilon_L$ as low as possible. From Eqs. (2.44) and (2.46), we have

$$\frac{\Delta \varepsilon_s}{\Delta \varepsilon_L} = \frac{2\alpha\beta\, b V_o \omega_c}{\omega E_1 \sinh \wedge z} \tag{2.51}$$

with $V_o = v_o^2 / 2\eta$, the beam voltage in the interaction region. Using Eqs. (2.20) and (2.23), the above can be written as

$$\frac{\Delta \varepsilon_s}{\Delta \varepsilon_L} = 2\beta b \sqrt{\frac{V_o I_o}{P_{e\ell}}} \frac{\omega_c}{\omega} \tag{2.52}$$

with $P_{e\ell} = P_{out} - P_{in}$. This form shows that the ratio of energy spread to mean energy loss decreases as the inverse square root of $P_{e\ell}$. Physically this is because the mean energy loss only begins to become sizable when

23

the beam has been displaced outward as a whole (i.e., it is second order in E_1), whereas <u>off axis</u> electrons gain or lose energy immediately on entrance into the interaction region, and result in a <u>spread</u> that is first order in E_1.

From Eqs. (2.20), (2.23) and (2.35), the RF power output can be expressed in terms of the beam displacement as

$$P_{e\ell} = P_{out} - P_{in} = \frac{1}{2} \omega B_o I_o \left| r_1(z) \right|^2 \tag{2.53}$$

Using this in Eq. (2.52), we find that an alternate expression for $\Delta \epsilon_s / \Delta \epsilon_L$ is

$$\frac{\Delta \epsilon_s}{\Delta \epsilon_L} = \frac{2b}{|r_1|} = \frac{\text{beam diameter}}{\text{beam displacement at output}} \tag{2.54}$$

This is a very appealing form, physically. It says that the filamentary beam picture – with very small $\Delta \epsilon_s / \Delta \epsilon_L$ – is applicable only when the RF beam motion is considerably larger than the actual beam size. If this is not the case, the distribution of longitudinal forces over the beam cross-section must be accounted for.

2.3.2 Cyclotron Wave Interaction

The above analysis has, of course, been concerned exclusively with the synchronous wave. For the cyclotron wave, a very similar analysis applies, and the longitudinal electric field at the beam has essentially the same form as that given above, except that now the field "seen" by an electron oscillates at approximately the cyclotron frequency since $\omega t - \beta z \simeq \omega_c t + \text{const.}$ following an electron. If

$$\frac{\alpha}{\beta_c} \ll \frac{\omega_p^2}{\omega_c^2} \quad , \tag{2.55}$$

24

as is generally the case, then the space-charge field dominates the energy spread generation, and the result is that energy spread with cyclotron wave interaction is smaller than with synchronous waves by a factor of ω_R/ω_c; i.e.,

$$\frac{\Delta \epsilon_s}{\Delta \epsilon_L} = \frac{2b}{|r_1|} \frac{\omega_R}{\omega_c}$$

$$= \frac{b}{|r_1|} \frac{\omega_p^2}{\omega_c^2} \tag{2.56}$$

for cyclotron wave interactions. In the above, the energy loss and energy spread referred to are only the axial kinetic energies. As mentioned in Section 2.2, for cyclotron waves the transverse kinetic energy is ω_c/ω times $\Delta \epsilon_L$, and any discussion of the efficiency with a depressed collector in this case would require an accounting of the transverse energy as well.

2.4 Design Considerations for High Efficiency Amplifiers

The most important result of the preceeding analysis is the prediction of a finite energy spread resulting from the finite beam size, as expressed by Eqs. (2.54) and (2.56). This energy spread places limits on the maximum theoretical efficiency obtainable with depressed collector operation (Eq. 2.50). High efficiency is of interest only for tubes of relatively high power, and high power implies a beam size of non-negligible dimensions. The purpose of this section is to summarize the main design equations, and to illustrate by a few examples what beam and circuit parameters are necessary for the achievement of a high efficiency power amplifier. We will concentrate exclusively on the synchronous wave amplifier in this discussion; design considerations for a cyclotron wave

25

amplifier are similar. (Our emphasis on synchronous wave devices is due to the fact that they have the potentiality of TWT type bandwidths).

2.4.1 Basic Design Equations

A summary of the basic design equations are given in Table I. The small signal gain (Eq. 2.23), the power output (derived from Eqs. (2.12) and (2.20)), and the minimum magnetic field for beam focusing (taken as twice the Brillouin field) are listed first. The expression for optimum efficiency with a depressed collector (Eq. 2.54) is given next. Since the optimum efficiency increases with increasing beam displacement, a theoretical limit can only be obtained when we limit the beam displacement (r_1). Our entire analysis has been confined to the small-signal regime, and therefore, we will only be able to give rough limits on the maximum beam displacement and the maximum efficiency.

There are several limits on the beam displacement or power output that must be considered. The first limit follows from the very gross statement that $\Delta\varepsilon_s + \Delta\varepsilon_L$ must remain less than V_o in the interaction region. From Eqs. (2.52) and (2.49), this implies that

$$\left(2\beta b \sqrt{\frac{\omega_c}{\omega} \frac{V_o I_o}{P_{e\ell}}} + 1 \right) \frac{P_{e\ell}}{I_o} < V_o \ . \tag{2.57}$$

Introducing the electronic efficiency (without depression)

$$\eta_e = \frac{P_{e\ell}}{V_o I_o} \ , \tag{2.58}$$

26

Equation (2.57) becomes

$$r_e + 2\beta b \sqrt{\frac{\omega_c}{\omega}} \; r_e^{1/2} < 1 \qquad (2.59)$$

The maximum value of η_e allowed by (2.59) is

$$(r_{e1})_{max} = \left[\left(1 + \frac{\omega_c}{\omega} \beta^2 b^2 \right)^{1/2} - \beta b \sqrt{\frac{\omega_c}{\omega}} \right]^2 \qquad (2.60)$$

and this is given as limit No. 1 in Table I. One should clearly be well below this limit for the analysis we have given to have any reasonable degree of validity; however, this limit can be (theoretically) approached only in cases of relatively large gain per wavelength (large α/β), as we will see in the examples.

A saturation mechanism that is usually far more important is the saturation of the growing wave by the reduction in the mean axial velocity due to the RF interaction. From the linear theory, the exponential growth ceases when the axial velocity is changed from the synchronous velocity by an amount

$$\left| \Delta v_z \right| = \frac{2\alpha v_o}{\beta} \qquad (2.61)$$

For small α/β, as usually obtained, this limit is reached for relatively small changes in the axial velocity. Since $P_{e\ell} \simeq v_o \Delta v_z I_o / \eta$, this predicts saturation effects when

$$\eta_e \simeq 4\alpha/\beta \qquad (2.62)$$

27

A detailed treatment of the nonlinear regime (See Section 3) shows that the _ultimate_ saturation in the output power occurs for $P_{e\ell}$ a factor of two to four times the limit in Eq. (2.62); in Table I we use a value of 8 α/β as the limit in η_e due to this effect. We should also point out that this limit could, in principle, be alleviated by tapering the phase velocity of the circuit (or the unperturbed beam velocity).

Another limit on the RF beam displacement is clearly that of interception by the circuit. The distance between the circuit and the beam should not be much larger than $1/\beta$, or the interaction impedance would be adversely affected. We therefore restrict the maximum value of βr_1 to a number the order of unity. This constraint is usually the least serious in the cases of interest to us, because of the relatively large magnetic field required for focusing a dense beam.

2.4.2 Some Typical Examples

With the relevant equations summarized in Table I, we now consider a few typical numerical cases. We use for illustration a tube operating at 3 GHz with a dc beam power of 10 kW (in the interaction region) in all cases. Since the largest beam displacement (smallest $\Delta\epsilon_s/\Delta\epsilon_L$) results with the smallest possible confining field, we use the minimum magnetic field in all examples. (We should caution the reader again that the numerical results on optimum efficiency that we give are to be viewed purely as rough estimates to serve as guidelines on the relative merit of the parameter choices; real accuracy should not be expected in view of the roughness of the nonlinear constraints that have been used).

In the first example (Table IIA), the _chosen_ beam parameters are 10 kV, 1 amp, and a current density of 10 A/cm^2 (moderately large area compression ratio). The beam radius is therefore 0.18 cm and the necessary magnetic field (twice the Brillouin value) is 900 gauss. For these parameters

28

Small signal gain $\qquad$ $\alpha = \beta \left[\dfrac{1}{2} \ \dfrac{I_o}{V_o} \ \dfrac{\omega}{\omega_c} \ K_t \right]^{1/2}$

Power output ($P_{out} \gg P_{in}$) $\qquad$ $P_{out} = \dfrac{1}{2} \ \omega I_o B_o \left| r_1 \right|^2$

Focusing $\qquad$ $\omega_c \overset{>}{\sim} 2\sqrt{2} \ \omega_p$

Optimum efficiency with
collector depression
(Valid only for η_e less than
limit #1) $\qquad$ $r_{opt} = \left(1 + \dfrac{\Delta\epsilon_s}{\Delta\epsilon_L} \right)^{-1}$

$\dfrac{\Delta\epsilon_s}{\Delta\epsilon_L} = \dfrac{2b}{r_1}$ (synchronous waves)

Saturation Limits on $\eta_e = P_{out}/V_o I_o$:

#1 "Reflected electrons" $\qquad$ $\eta_e < \left[(1 + A^2)^{1/2} - A \right]^2$
$\quad$ ($\Delta\epsilon_s + \Delta\epsilon_L < V_o$)

$\qquad\qquad\qquad\qquad\qquad\quad A = \beta b \sqrt{\dfrac{\omega_c}{\omega}}$

#2 Velocity desynchronization $\qquad$ $\eta_e \overset{\sim}{<} 8\alpha/\beta$

#3 Beam interception $\qquad$ $\beta r_1 < 1$

TABLE I

Design Equations for Transverse-Wave Amplifier

29

Examples of Calculated Performance
of Synchronous-Wave Amplifiers

J_o = 10 amps/cm^2	b = 0.18 cm (beam radius)		
V_o = 10 kV	B_o = 900 gauss		
I_o = 1 amp	Saturation limit #1:		
f = 3 GHz	η_e < 35%		
	Interaction Impedance (K_t)		
	100Ω	10Ω	1Ω
$3/\alpha$ = length for 20 dB gain	12 cm	38 cm	120 cm
η_{e2} = 8 α/β	62 %	20 %	6.2 %
P_{out} maximum	(1) 3.6 kW	2 kW	620 kW
βr_1 at maximum P_{out}	0.67	0.5	0.15
η_{opt}	(1) < 35%	30%	10 %

(1) limited by saturation mechanism #1.

| J_O = 25 amps/cm^2 | | | b = 0.11 cm (beam radius) | | |

	Interaction Impedance (K_t)		
J_O = 25 amps/cm^2	b = 0.11 cm (beam radius)		
V_O = 10 kV	B_O = 1.45 kilogauss		
I_O = 1 amp	Saturation limit #1:		
f = 3 GHz	η_e < 46%		
	Interaction Impedance (K_t)		
	100Ω	10Ω	1Ω
$3/\lambda$ = length for 20 dB gain	10 cm	60 cm	190 cm
η_{e2} = 8 α/β	40%	13 %	4 %
P_{out} maximum	4 kW	1.3 kW	400 W
βr_1 at maximum P_{out}	0.5	0.3	0.16
η_{opt}	42 %	30 %	18 %

Examples of Calculated Performance
of Synchronous–Wave Amplifiers

TABLE IIC

J_O = 25 amps/cm^2	b = 0.08 cm (beam radius)	
V_O = 20 kV	B_O = 1.2 kilogauss	
I_O = 0.5 amps	Saturation limit #1:	
f = 3 GHZ	$n_e < 70\%$	
	Interaction Impedance (K_t)	
	100 Ω	10 Ω
$3/\alpha$ = length for 20 dB gain	40 cm	120 cm
n_{e2} = $8\alpha/\beta$	28 %	8 %
P_{out} maximum	2.8 kW	800 W
βr_1 at maximum P_{out}	0.50	0.26
n_{opt}	56 %	41 %

Examples of Calculated Performance
of Synchronous-Wave Amplifiers

saturation constraint No. 1 limits us to an ultimate efficiency of much less than 35%. At the bottom of Table IIA, the interaction length required for approximately 20 dB gain is given as a function of the circuit interaction impedance, along with the other relevant quantities. We note that an interaction impedance of 10 ohms or greater is necessary to keep the length of the tube within reasonable bounds. With such an interaction impedance saturation limit No. 1 imposes the most severe constraint, and efficiencies in excess of 20% are very unlikely in this case.

In Table IIB, we have increased the current density to 25 A/cm^2 without changing the voltage or net current to see the effect of a reduced beam diameter. The overall conclusion is that the necessary increase in the focusing magnetic field largely offsets any dramatic improvements in the predicted performance.

The final example is presented in Table IIC. We retained the higher current density and went to a much higher beam impedance (20 kV, 1/2 amp). The higher beam impedance means that a higher interaction impedance is necessary to keep the tube length within reasonable bounds, but with the higher interaction impedance ($\sim$ 100 ohms), rather good optimum efficiencies (56%) are predicted. The "gross" saturation constraint (#1) has been moved up to $\eta_e \approx$ 70%, so we are well below this limit with this design.

2.4.3 Scaling Laws

The numerical examples listed in Table II give us an idea of the efficiency obtainable with transverse wave interactions. We now briefly consider how the optimum efficiency results scale with the chosen parameters such as frequency, beam voltage, etc. The "best" design would of course satisfy many criteria besides optimization of the efficiency (bandwidth, tube length, etc.), but we concentrate solely on this parameter in the present section.

33

If we choose as independent parameters f, J_o, V_o, η_e, and P_{out} (the RF output power), then $I_o = P_{out}/\eta_e V_o$, $b^2 = I_o/\pi J_o$, and the minimum B_o is fixed according to the focusing constraint in Table I. The resulting energy spread scales as

$$\frac{\Delta\epsilon_s}{\Delta\epsilon_L} \sim \frac{f^{1/2} P_{out}^{1/2}}{\eta_e V_o^{9/8} J_o^{1/4}}$$

This illustrates that the attainment of high efficiencies with collector depression is more difficult at high powers and high frequencies. We can also see that higher voltages are better, the basic reason being the fact that higher power can then be obtained with less current. (This trend, of course, has a practical upper limit since the tube length would become prohibitively long for very large V_o/I_o). We can also see that although a higher current density reduces $\Delta\epsilon_s$, the improvement only goes as the 1/4 power of J_o.

If we now take the electronic efficiency to be limited by mechanism #2 in Table I, and choose K_t, f, J_o, V_o, and P_{out} as the independent parameters, the energy spread scales as

$$\frac{\Delta\epsilon_s}{\Delta\epsilon_L} \sim \frac{f^{1/6} P_{out}^{1/6}}{V_o^{13/24} J_o^{1/12} K_t^{1/3}}$$

Note the very weak dependence on <u>all</u> parameters in this case. This result illustrates that in the domain where η_e is limited by the axial velocity desynchronization, very little improvement could be achieved by methods such as beam compression (increased J_o) or increases in the interaction impedance.

34

2.5   Conclusion

The original suggestion of high-efficiency from transverse-wave interactions was based on the analysis of a filamentary beam. Under practical conditions, the filamentary beam model is inadequate for the description of a tube designed for a reasonably high power output, because high power can be obtained only with a beam of finite cross-section and non-negligible space charge. In this section we presented a quantitative analysis of the effects of finite beam size and space charge on the RF-induced velocity spread. The summary of design equations and numerical examples cited in Section 2.4 show that the optimum efficiency attainable in a synchronous-wave device is indeed limited by these considerations. The longitudinal energy spread in a cyclotron-wave amplifier should be much less than in synchronous-wave devices according to the result obtained in Section 2.3.2. In cyclotron-wave devices, however, the electron beam acquires a sizable transverse kinetic energy that must be accounted for in the design of depressed collectors for high-efficiency operation.

The main conclusion of our study is that efficiencies in excess of 50% with output powers in excess of a kilowatt are theoretically possible in a transverse-wave tube; however, a rather substantial area compression of the beam would be necessary as well as a relatively high beam impedance (V_o/I_o). Without this careful attention to the minimization of beam size, our theory predicts that the efficiency of transverse wave tubes would probably be no better than is presently obtainable with ordinary TWT's.

III.   NONLINEAR BEHAVIOR OF TRANSVERSE-WAVE AMPLIFIERS

3.1   Introduction

The theoretical analysis presented in Section 2 is a small-signal theory in the sense that changes in the axial velocity, ΔV_z, are assumed small enough that the phase synchronous condition $(\omega \simeq \beta V_z)$ can be maintained over the entire length of the interaction region. As we have seen in the previous section, however, the amplification of the wave takes place at the expense of the longitudinal beam velocity, and, therefore, one would expect a saturation mechanism due to the reduction in the mean axial velocity of the beam. In Section 2.4, we estimated the threshold of this saturation mechanism by specifying an allowable velocity spread, $(\Delta v_z = 2\alpha v_o/\beta)$. We would expect the small-signal theory to begin to fail, when the percentage energy lost by electrons exceed a number of the order of (α/β). This limitation could be a severe one, since (α/β) is typically of the order of few percent.

The nonlinear theory presented here accounts for the loss of synchronism due to extended interactions and can quantitatively predict how the output power of the tube saturates at high input drive levels. In marked contrast to the nonlinear theories of ordinary traveling-wave tubes[18], we are able to develop a rather complete analytical nonlinear theory of the transverse-wave tube. The basic reason for this relative simplicity derives from the fact that, in our case, all electrons have a similar "history" in traveling through the circuit, "scrambling" in phase and overtaking does not occur as readily in a transverse wave tube as it does with space-charge wave interactions.

In Section 3.2, we derive nonlinear interaction equations. For the sake of completeness, some of the basic equations presented in Section 2 are repeated in Section 3.2. The final result of the development in

36

Section 3.2 is the nonlinear differential equation for the amplitude of the wave in a transverse-wave traveling-wave amplifier. In Section 3.3, we examine the behavior of the amplifier in various limiting cases, we obtain approximate solutions to the nonlinear equations. In Section 3.4, we present results of numerical calculations to show the saturation characteristics and the effect of over-voltaging on the power output.

3.2 Derivation of Nonlinear Equations

The basic assumptions in the analysis are the following:

1. The filamentary beam model is used throughout. An analysis of the axial energy spread resulting from finite beam size in the small-signal regime has been given in Section 2. If the RF displacement exceeds the beam diameter, this model should be reasonably accurate.

2. The displacement of the beam from the axis is assumed to be much less than $1/\beta$, so that the amplitude of the transverse circuit field is essentially constant in the region of interest. This assumption should be well satisfied in almost all cases of interest.

3. The percentage change in axial velocity is assumed to be relatively small even up to saturation. As will be shown, this approximation is reasonable as long as the small-signal gain per wavelength $(\frac{\alpha}{\beta})$ is relatively small; this limit should cover the majority of the cases of interest.

4. The circuit is assumed to be lossless.

3.2.1 Basic Description of the Beam-Circuit Interaction

For analytical convenience, we use the circularly-polarized variables introduced in Section 2.

$$r = x + jy \tag{3.1}$$

$$E_c = E_x + jE_y \tag{3.2}$$

where $x(z,t)$ and $y(z,t)$ describe the beam position, and E_x and E_y are the transverse components of the circuit field at the beam position. The transverse component of the force equation can then be written as

$$\frac{d^2 r}{dt^2} - j\omega_c \frac{dr}{dt} = -\eta E_c \tag{3.3}$$

with $\eta = |e|/m$ and $\omega_c = \eta B_o$, with B_o the unperturbed axial magnetic field in the $+z$ direction. We will confine our attention here to the synchronous wave; in Appendix A we show that the final results have exactly the same form for the cyclotron wave interaction. For synchronous wave interactions, we can take $|dr/dt| << \omega_c r$ and drop the first term on the left side of Eq. (3.3). Physically, this assumption means that we have taken the time variation of the electric field in the beam frame to be slow, so that the electron motion follows the usual adiabatic law, $\bar{v} = \bar{E} \times \bar{B}_o / B_o^2$.

The time dependence of E_c is now taken as $e^{j\omega t}$; higher harmonics induced on the circuit are assumed to be negligible. It is shown below that the axial velocity (v_z) is a function of z alone, and therefore, the beam displacement has the same time dependence $\left[r(z,t) = r(z)\, e^{j\omega t} \right]$. The transverse equation of motion is therefore

$$\left(\frac{\partial}{\partial z} + \frac{j\omega}{v_z} \right) \; r = \frac{-j\eta}{\omega_c v_z} \; E_c \tag{3.4}$$

38

The beam is assumed to be weakly coupled to the circuit, so
that the differential equation for the (right-circularly polarized) circuit
mode can be written as

$$\frac{\partial E_c}{\partial z} + j\beta_o E_c = cr \qquad (3.5)$$

where β_o is the "cold" propagation constant of the circuit mode, and "c"
is a coupling constant that will be evaluated below from power conservation
considerations.

In a linear analysis, we would take $v_z \simeq v_o$, the injection
velocity. For the nonlinear theory, we must determine v_z from

$$\frac{dv_z}{dt} = -\eta E_{zb} \qquad (3.6)$$

where E_{zb} is the longitudinal field <u>at the beam position.</u> Because of
assumption (2), we can write

$$E_{zb} \simeq \frac{\partial E_z}{\partial x} x + \frac{\partial E_z}{\partial y} y \qquad (3.7)$$

For slow waves, $\nabla \times \bar{E} \simeq 0$ and the above becomes

$$E_{zb} = \frac{\partial E_x}{\partial z} x + \frac{\partial E_y}{\partial z} y$$

$$= \mathrm{Re}\left(r \frac{\partial E_c}{\partial z}^*\right) \simeq \mathrm{Re}\,(j\beta_o r E_c^*) \qquad (3.8)$$

39

The time-average power carried by the circuit is defined as

$$P_c = \frac{|E_c|^2}{2\beta_o^2 K_t} \tag{3.9}$$

in terms of the (transverse) interaction impedance, K_t. Since the transverse kinetic energy of the electrons is small in a synchronous-wave interaction, conservation of energy requires

$$\frac{\partial P_c}{\partial z} = |I_o| \, E_{zb} \tag{3.10}$$

where $|I_o|$ is the magnitude of the unperturbed beam current. This relation follows by noting that $-\partial P_c/\partial z$ must be the power per unit length given to the electrons, which is $(-e\bar{v} \cdot \bar{E}) \lambda_o = -|I_o| \, E_{zb}$ where λ_o is the number of electrons per unit length. (For cyclotron waves, the transverse kinetic energy of the electrons must also be included, in the energy balance, as is shown in Appendix A).

To evaluate the coupling constant c in Eq. (3.5), we note that

$$\frac{\partial}{\partial z} |E_c|^2 = crE_c^* + c^* r^* E_c \tag{3.11}$$

or

$$\frac{\partial}{\partial z} P_c = \frac{1}{\beta_o^2 K_t} \, \mathrm{Re}(crE_c^*) \tag{3.12}$$

40

From Eq. (3.10) and Eq. (3.8), we see that

$$\frac{\partial P_c}{\partial z} = \left| I_o \right| \, \mathrm{Re} \, (j\beta_o r E_c^{\,*}) = \beta_o r \left| I_o \right| \left| E_c \right| \tag{3.13}$$

A comparison of (3.12) and (3.13) shows that

$$C = j\beta_o^3 \, K_t \left| I_o \right| \tag{3.14}$$

It is convenient to remove the "fast" variation in E_c by defining

$$E_c(z) = \widetilde{E}(z) \, e^{-j\beta_o z} \tag{3.15}$$

Equation (3.5) becomes

$$r = \frac{1}{c} \, e^{-j\beta_o z} \, \frac{\partial \widetilde{E}}{\partial z} \tag{3.16}$$

A single differential equation for $\widetilde{E}$ is then obtained by using Eq. (3.16) in Eq. (3.4);

$$\frac{\partial^2 \widetilde{E}}{\partial z^2} + j \left(\frac{\omega}{v_z} - \beta_o \right) \frac{\partial \widetilde{E}}{\partial z} - \alpha_o^2 \widetilde{E} = 0 \tag{3.17}$$

with

$$\alpha_o^2 = \frac{\eta \beta_o^3 \left| I_o \right| K_t}{\omega_c v_z} \tag{3.18}$$

All of the usual small-signal results are obtained from Eq. (3.17) by taking $v_z \simeq v_o$, the unperturbed velocity. This is allowed in a small-signal theory since the longitudinal field is second order in the perturbation amplitude.

To calculate the change in the longitudinal velocity, it is important to note that the longitudinal electric field at the beam given by Eq. (3.8) <u>is a function of z only</u>, and is not explicitly a function of time even though r and E_c both vary as $e^{j\omega t}$.

Therefore, $v_z = v_z(z)$ and Eq. (3.6) becomes

$$v_z \frac{\partial v_z}{\partial z} = -\eta E_{zb}(z)$$
$$= - \frac{\eta}{|I_o|} \frac{\partial P_c}{\partial z} \tag{3.19}$$

We can integrate (3.19) to obtain

$$\frac{1}{2}(v_z{}^2 - v_o{}^2) = - \frac{\eta}{|I_o|}(P_c - P_{in}) \tag{3.20}$$

where v_o is the velocity at the injection point, and P_{in} is the input circuit power.

To calculate $P_c(z)$, we must solve Eqs. (3.17) and (3.20) siumltaneously. This could be done numerically, but it turns out that in the spirit of the weak coupling assumptions that underlie our basic equations $(\alpha_o << \beta)$, the interaction will saturate for $|v_z - v_o|/v_o << 1$. Therefore,

42

we can approximate (3.20) as

$$v_1 = -\frac{\eta}{|I_o| \, v_o} (P_c - P_{in}) \qquad (3.21)$$

where $v_1 = v_z - v_o$, and we note that the only important place in Eq. (3.17) where v_1/v_o must be kept is in the term

$$\frac{\omega}{v_z} - \beta_o \simeq \frac{\omega}{v_o} - \beta_o - \frac{\omega}{v_o^2} v_1 \qquad (3.22)$$

since $(\omega/v_o - \beta_o)$ will be very small (the order of α_o) in all cases of interest. We also note that α_o can be treated as a constant in this approximation, and Eq. (3.18) can be written in the form

$$\alpha_o^2 \simeq \beta_o^2 \; \frac{1}{2} \; \frac{\omega}{\alpha_c} \; \frac{I_o}{V_o} \; K_t \qquad (3.23)$$

with $\frac{1}{2\eta} v_o^2 = V_o$.

3.2.2 Normalized Equation for the Circuit Power vs. Distance

The basic differential equation for $\widetilde{E}$ (Z) is given by Eq. (3.17), with the change in axial velocity (v_1) given in Eq. (3.21). We introduce a normalized circuit field amplitude

$$\cdot (z) = \widetilde{E} \, (z)/E_{in} \qquad (3.24)$$

with E_{in} the complex amplitude of the circuit field at the input $(Z = 0)$. A normalized distance (ζ) is defined as

$$\zeta = \alpha_o z \qquad (3.25)$$

Equation (3.17) then becomes

$$\frac{d^2 \hat{\mathcal{E}}}{d\zeta^2} + j \left[4Q \left(|\hat{\mathcal{E}}|^2 - 1 \right) - 2\delta \right] \frac{d\hat{\mathcal{E}}}{d\zeta} - \hat{\mathcal{E}} = 0 \qquad (3.26)$$

where

$$Q = \frac{1}{4} \frac{\omega \eta P_{in}}{I_o v_o^3 \alpha_o} \simeq \frac{\beta_o}{\alpha_o} \frac{P_{in}}{3 V_o I_o} \qquad (3.27)$$

and

$$\delta = \frac{1}{2} \frac{(\beta_o - \omega/v_o)}{\alpha_o} \qquad (3.28)$$

The dimensionless quantity "Q" expresses the input drive level, and δ is determined by the "detuning" of the beam voltage V_o away from perfect synchronism at the input $(\delta = 0)$. The boundary conditions on $\hat{\mathcal{E}}(\zeta)$ at $\zeta = 0$ are

$$\hat{\mathcal{E}}(0) = 1 \qquad (3.29)$$

$$\frac{d\hat{\mathcal{E}}}{d\zeta}(0) = 0 \qquad (3.30)$$

44

The latter condition follows from Eq. (3.16), since the beam is assumed to enter the circuit unmodulated $(r(0) = 0)$.

We now express the complex field amplitude $\mathcal{E}(\zeta)$ in terms of its magnitude and phase as

$$\mathcal{E}(\zeta) = A(\zeta)\, e^{j\theta(\zeta)} \tag{3.31}$$

Substituting this form into Eq. (3.26), we obtain the following coupled differential equations for A and θ.

$$A'' - \left[(\theta')^2 + 1 \right] A - \theta' A \left[4Q(A^2 - 1) - 2\delta \right] = 0 \tag{3.32}$$

$$\theta'' A + 2\theta' A' + \left[4Q(A^2 - 1) - 2\delta \right] A' = 0 \tag{3.33}$$

(In the above, we have used the shorthand notation $A' = dA/d\zeta$, etc.)

Since Eq. (3.33) is a first-order equation in θ', we can solve for θ' in terms of A as

$$\theta'(\zeta) = -\frac{1}{A^2} \int_0^\zeta \left\{ 4Q\left[A^2(\zeta) - 1 \right] - 2\delta \right\} A(\zeta)\, A'(\zeta)\, d\zeta$$

$$= -\frac{(A^2 - 1)}{A^2} \left[Q(A^2 - 1) - \delta \right] \quad , \tag{3.34}$$

where we have used the fact that the boundary condition (3.30) requires $\theta'(0) = 0$ and $A(0) = 1$.

A differential equation for A alone can be obtained by using Eq. (3.34) in Eq. (3.32). The resulting equation can be integrated once by multiplying by A'. We can derive the final result much faster by

using the following relation that is easily derived from Eq. (3.26).

$$\frac{d}{d\zeta} \left| \dot{\cdot} \right|^2 - \frac{d}{d\zeta} \left| \zeta \right|^2 = 0 \tag{3.35}$$

This yields, upon one integration,

$$\left(\frac{dA}{d\zeta}\right)^2 + (\theta')^2 A^2 = A^2 - 1 \tag{3.36}$$

If we now use Eq. (3.34) in this relation (rather than in Eq. (3.32)), we obtain the following first-order differential equation for $A(\zeta)$.

$$\left(\frac{dA}{d\zeta}\right)^2 = (A^2 - 1) \left\{ 1 - (1 - \frac{1}{A^2}) \ (QA^2 - Q - \delta)^2 \right\}$$

$$\equiv F(A) \tag{3.37}$$

The calculation of the normalized circuit field amplitude $A(\zeta)$ (and also the phase $\theta(\zeta)$, if desired) has thus been reduced to a quadrature, since

$$\zeta = \int_1^A \frac{dA_1}{\sqrt{F(A_1)}} \tag{3.38}$$

An alternate form for this integral results when we change variables to $u = (A^2 - 1)^{1/2}$.

$$\zeta = \int_0^{(A^2 - 1)^{1/2}} \frac{du}{\left[1 + u^2 - u^2 \ (Qu^2 - \delta)^2 \right]^{1/2}} \tag{3.39}$$

46

This form is preferred for numerical computation, since it eliminates the (integrable) divergence of the integrand at the lower limit.

3.3   General Discussion of the Saturation Characteristics; Approximate Solutions

The growth of the normalized circuit field amplitude (A) or power $(P_c(z)/P_{in} = A^2)$ as a function of distance is governed by Eqs. (3.37) -(3.39). In the remainder of this section, we will be concerned with the solutions to these basic equations. For the reader's convenience, we remark again that the distance has been normalized as in Eq. (3.25) where α_o is the small-signal gain constant (c.f., Eq. 3.23), Q is the normalized input power level (Eq. 3.27), and δ is a normalized variable expressing the shift of the beam voltage away from perfect synchronism (Eq. (3.28). (In the following we will not be concerned with the effects of nonlinearities on the output phase; however, this quantity could be calculated from Eq. (3.34) if desired).

In the present section we will discuss the general characteristics of the nonlinear behavior and some approximate analytical solutions, while in the following section we present results of a numerical integration of Eq. (3.39) for several cases of interest.

3.3.1   Small-signal Limit

We consider first the small-signal limit to illustrate how the well-known linear results are obtained from our general formulation. In the limit $Q \to 0$, Eq. (3.39) becomes

$$\zeta = \int_0^{(A^2 - 1)^{1/2}} \frac{du}{\left[1 + (1 - \delta^2) \, u^2 \right]^{1/2}} \qquad (3.40)$$

47

This integral can be performed analytically; for $\delta^2 < 1$ the result is

$$\zeta = \frac{1}{(1 - \delta^2)^{1/2}} \sinh^{-1} \left[(1 - \delta^2)(A^2 - 1) \right]^{1/2} \qquad (3.41)$$

An explicit expression for $A(\zeta)$ can therefore be obtained in this case. For $\delta^2 < 1$, we have

$$A^2 = \frac{P_c(z)}{P_{in}} = 1 + \frac{\sinh^2(\sqrt{1 - \delta^2}\ \zeta)}{(1 - \delta^2)} \qquad (3.42)$$

and with $\delta^2 > 1$,

$$A^2 = 1 + \frac{\sin^2(\sqrt{\delta^2 - 1}\ \zeta)}{(\delta^2 - 1)} \qquad (3.43)$$

A sketch of A^2 as a function of ζ is presented in Fig. 5 for several values of δ. Note that all of the curves start out with an initial growth $A^2 \sim 1 + \zeta^2$; if $|\delta| < 1$ then we are in the region of exponential growth with z, and it is clear from Eq. (3.42) that the fastest rate of growth is <u>at</u> synchronism $(\delta = 0)$. If $|\delta|$ is <u>greater</u> than one, then the circuit wave amplitude oscillates periodically with z, as indicated in Fig. 5. For δ significantly greater than unity, there is very little energy exchange between the beam and the circuit, as would be expected physically.

3.3.2 General Characteristics of Nonlinear Saturation; Efficiency of a High Gain Amplifier
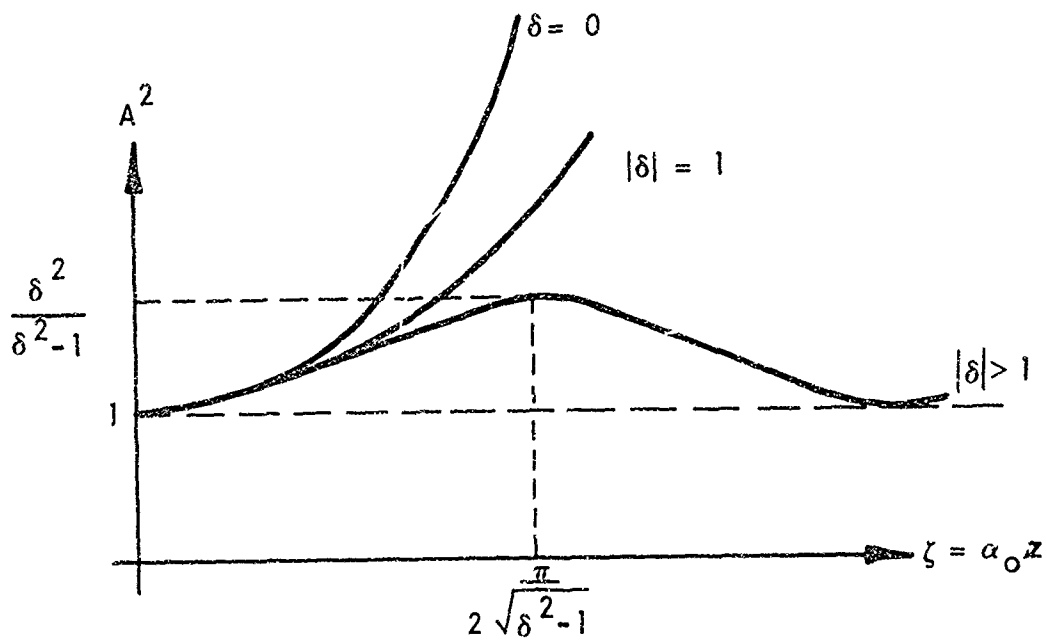
In the linear analysis discussed above, we set $Q = 0$

48

FIGURE 5 A^2 VS ζ IN THE SMALL-SIGNAL LIMIT (Q=0)

in Eq. (3.37); this approximation clearly breaks down when A^2 becomes large enough to make QA^2 the order of unity. With nonzero A, the general shape of the A^2 vs. ζ curve must be as shown in Fig. 6. The reasoning is as follows. Initially, A increases with ζ since $dA/d\zeta = \sqrt{F}$ is positive. It is clear from Eq. (3.37), however, that F must become negative for sufficiently large A, and therefore a "saturation" amplitude (A_s) must exist for which $dA/d\zeta = \sqrt{F(A_s)} = 0$. At this point the amplitude is a maximum; beyond this point it decreases since $d^2 A/d\zeta^2$ can be shown to be negative at $A = A_s$. The overall behavior of A vs. ζ is therefore oscillatory, as shown in Fig. 6. The existence of this oscillatory behavior can also be easily appreciated by noting the analogy between Eq. (3.37) and a nonlinear mass-spring oscillator or with the motion of a particle in a potential well $\left[(dx/dt)^2 = E - V(x) \right]$.

From Eq. (3.37), the equation determining the saturation amplitude is

$$\left[Q(A_s^2 - 1) - \delta \right]^2 \ (1 - 1/A_s^2) = 1 \tag{3.44}$$

Equation (3.44) can have several real roots for A_s^2, and clearly the smallest real root is the one of interest. For $\delta = 0$, and with a "high gain" amplifier, saturation will occur for $P_{out} \gg P_{in}$ (or $A_s \gg 1$). In this case, we have

$$QA_s^2 \simeq 1 \tag{3.45}$$

or

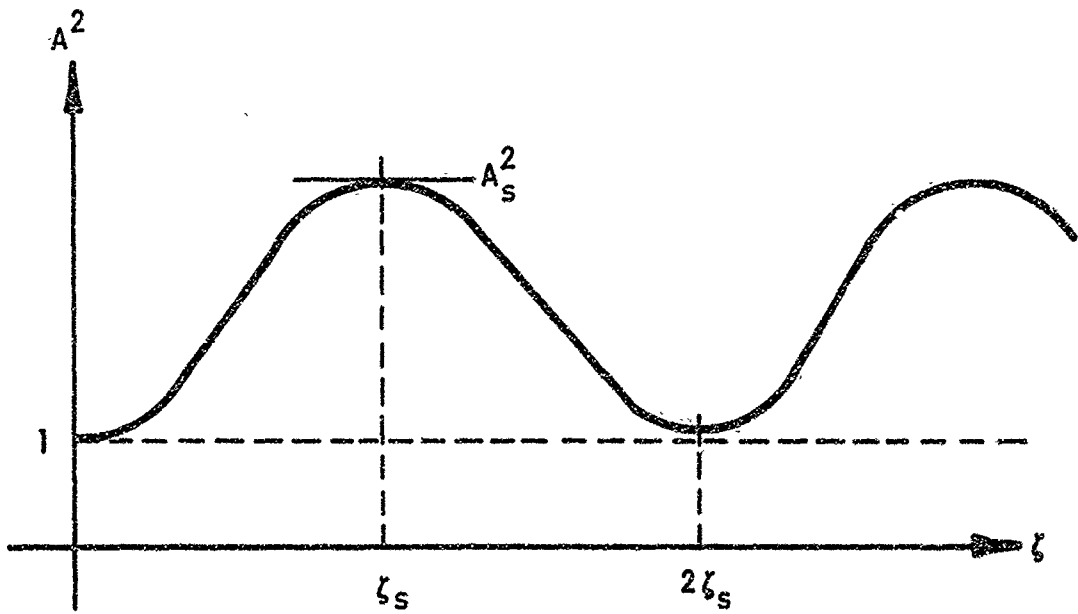$$(P_{out})_{max} \approx \frac{8 \nu_o}{\beta_o} \ V_o I_o \tag{3.46}$$

FIGURE 6   GENERAL STRUCTURE OF THE NONLINEAR SOLUTION
FOR A (ζ)

D-9322

The maximum electronic efficiency of such a high gain amplifier, when operated <u>at</u> the synchronous voltage, is $8\sigma_o/\beta_o$.

The order of magnitude of this saturation level of the output power can be obtained directly from the small-signal equations by evaluating how much axial energy can be taken from the beam before the gain constant drops to zero. From this physical picture of the saturation mechanism, we would expect that an improvement in the efficiency could be realized by over-voltaging the tube somewhat (making $\delta > 0$), since then the beam could lose more axial energy before it slips out of synchronism with the circuit. This is indeed the case, since the approximate solution of Eq. (3.44) for A_s with $A_s \gg 1$ and $\delta \neq 0$ is

$$QA_u^2 = 1 + \delta \tag{3.47}$$

which indicates an improvement in the maximum output power by a factor of $(1 + \delta)$. Of course, we would expect some sort of limit on how much this improvement can be (i.e., how big δ can be), since the linear analysis indicates that very little energy exchange between the beam and circuit occurs for $\delta \gg 1$. The complete answer to this question must await the numerical studies in Section 3.4. We can, however, make a few general comments about the $Q \ll 1$ limit, which adequately covers the "high gain" case. (By "high gain" we mean not only large small-signal gain, but also $P_{out} \gg P_{in}$ under saturation conditions as well).

The key question is to determine whether or not Eq. (3.47) is the <u>smallest</u> real root of Eq. (3.44). To answer this question, we define

$$\Psi = A^2 - 1 \tag{3.48}$$

52

and

$$G = \frac{A^2}{A^2 - 1} \, F(A)$$

$$= \Psi + 1 - \Psi (Q\Psi - \delta)^2 \tag{3.49}$$

The general shape of G vs. Ψ is illustrated in Fig. 7. With $\delta \leq 0$, $G(\Psi)$ has only one zero for $\Psi > 0$. For $\delta > 0$, a critical value of δ exists where three real roots for Ψ appear. At this critical value of δ, we have $G = 0$ and $\partial G / \partial \Psi = 0$ (see Fig. 7). If we again concentrate on a high gain amplifier ($Q \ll 1$ and $\Psi_c \gg 1$), the onset of the real root at $\Psi = \Psi_c$ occurs for

$$\Psi_c \approx \frac{1}{\sqrt{2Q}} \tag{3.50}$$

and

$$\delta_c = 1 + \sqrt{\frac{Q}{2}} \tag{3.51}$$

From this analysis, the maximum value of A_s^2 as a function of δ (for $Q \ll 1$) occurs for $\delta \approx 1$, and therefore the maximum possible electronic efficiency of a high gain amplifier is

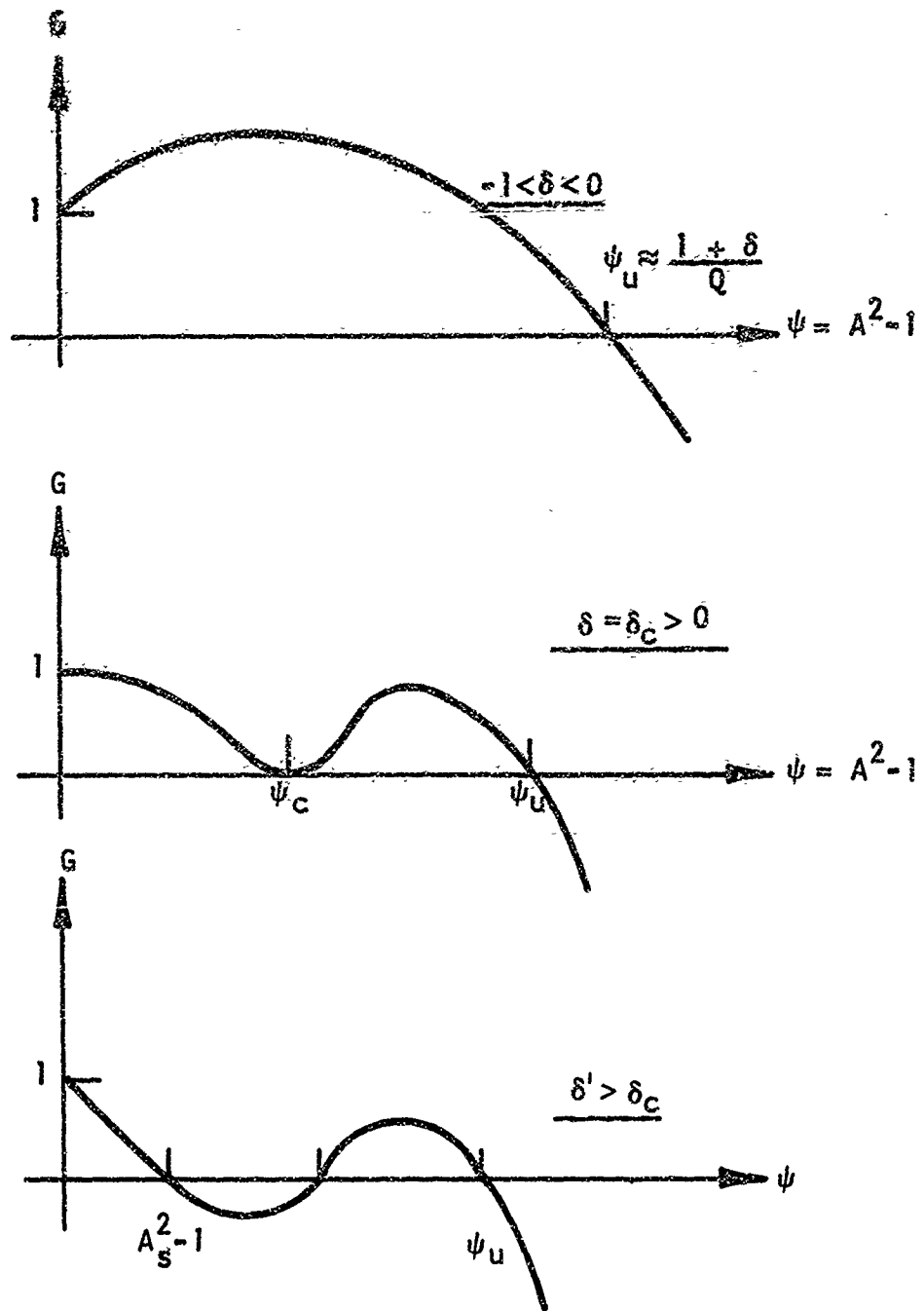$$(\eta_{e\ell})_{max} = \frac{P_{out}}{V_o I_o} = 16 \frac{\alpha_o}{\beta_o} \tag{3.52}$$

53

FIGURE 7   SKETCH OF G VS ψ TO DETERMINE THE REAL ROOTS OF
G=0 (of F=0) AS A FUNCTION OF δ FOR Q<<1

D-9321

3.3.3 Approximate Solution of the Nonlinear Equations for
a High Gain Amplifier Operated at Initial Synchronism

In this section we develop an approximate solution to Eq. (3.39) for the case $\delta = 0$ and $Q \ll 1$. As noted in the preceeding section, "saturation" occurs for $QA^2 \sim 1$ and therefore a high gain amplifier $(A_{out} \gg 1)$ will saturate when Q is still much less than unity.

We let

$$u = \sinh \gamma \tag{3.53}$$

in Eq. (3.39); the integation then becomes

$$\zeta = \int_0^{\cosh^{-1} A} \frac{d\gamma}{\left[1 - \frac{(\sinh \gamma)^6}{(\cosh \gamma)^2} Q^2\right]^{1/2}} \tag{3.54}$$

As long as $Q \ll 1$, we can use

$$Q^2 \frac{(\sinh \gamma)^6}{(\cosh \gamma)^2} \simeq \frac{Q^2}{16} e^{4\gamma} \tag{3.55}$$

since this term is negligible compared to unity unless $\gamma \gg 1$. We then obtain

$$\zeta = \gamma_0 - \frac{1}{4} \ln \frac{1}{2} \left(1 + \sqrt{1 - \frac{Q^2}{16} e^{4\gamma_0}}\right) \tag{3.56}$$

where

$$\gamma_0 = \cosh^{-1} A \tag{3.57}$$

55

Equation (3.56) gives ζ (A) in a readily calculable form; we should also point out that this equation is only valid in the region $\zeta \leq \zeta_s$ since the positive square root of F was used in deriving (3.39) from (3.37).

From Eq. (3.56), we see that saturation occurs when $\gamma_o = \gamma_{om}$, where

$$\frac{Q}{4} e^{2\gamma_{om}} = 1$$

or

$$A_s^{\;2} = (\cosh \gamma_{om})^2 \approx 1/Q$$

in agreement with the results of Section 3.3.2. The saturation distance is given by

$$\zeta_s = \frac{1}{2} \, \ell n \, \frac{4\sqrt{2}}{Q}$$

As an example, the A^2 vs. ζ curve is given in Fig. 8. for the case $Q = 10^{-2}$.

3.4   Numerical Solutions of the Saturation Characteristics

In this section we will present the results of a numerical integration of the nonlinear equation of motion, Eq. (3.39). Most of the approximate analytical results in the previous section are restricted to the "high-gain regime" $(A^2 \gg 1)$. In the present section our main emphasis will be on the "intermediate" gain regime where the analytical results fail.

To determine the output power as a function of the input drive power (Q) and beam voltage tuning (δ), we used a numerical integration
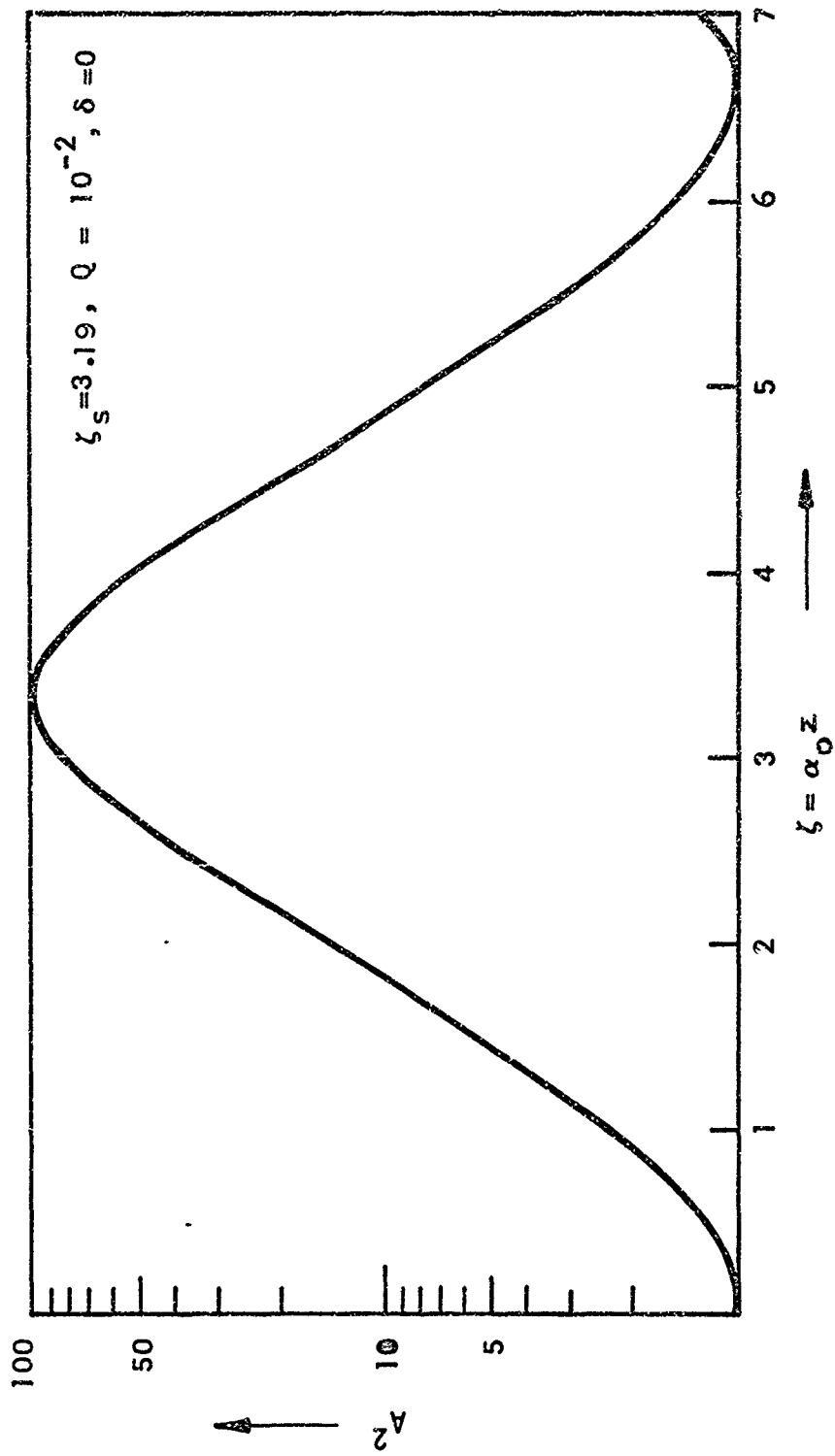
56

FIGURE 8 GAIN VS NORMALIZED DISTANCE (SMALL-SIGNAL LIMIT)

$\zeta_s = 3.19$, $Q = 10^{-2}$, $\delta = 0$

$\zeta = \alpha_0 z$

A^2

57

D-9320

routine to evaluate Eq. (3.39), giving sets of values of A^2 and ζ (for particular Q and δ inputs) up to the saturation position ζ_s where the denominator of Eq. (3.39) vanishes. Beyond this point, we used the periodicity of the A vs. ζ relation, so that only the $\zeta \leq \zeta_s$ region needs to be calculated explicitly. Repeating the numerical integration for a variety of Q and δ values allows us to construct curves of output power vs. input drive for a given tube length and a given beam voltage (see Figs. 9 and 10).

The case of an interaction length $l = 2/\alpha_o$ is shown in Figs. 9 and 10. In Fig. 9 the gain ($A^2 = P_{out}/P_{in}$) as a function of input drive level is presented, while in Fig. 10 the same results are presented in the form of net electronic power conversion efficiency $(P_{out} - P_{in})/P_o$ vs. input drive.

With the beam voltage precisely at synchronism ($\delta = 0$), the maximum power conversion efficiency is obtained at $Q \sim 0.1$, and the power gain is about 11 at this maximum. (compared to a small signal power gain of 15). (At saturation, $Q(A^2 - 1)$ is very close to unity, in agreement with the predictions of Section 3.3.2). Note the regime $Q \gg 1$ in Fig. 9 where the gain is zero at certain input drive levels. These nulls arise when Q is such that tube length is an even multiple of ζ_s (Q) (see Fig. 5), while the "peaks" occur when the length is an odd multiple of ζ_s.

The saturation characteristics of an "over-voltaged tube" ($\delta > 0$) are shown in Figs. 9 and 10. With $\delta = 1$, saturation occurs for $Q \sim 0.25$ and the maximum electronic power output is doubled compared to the synchronous case, in good agreement with the preceeding "large gain" theory (c.f. Eq. 3.47). To achieve this higher electronic efficiency, we must sacrifice a certain amount of gain ($A_s^2 \sim 9$ at $\delta = 1$ and $Q = .25$).
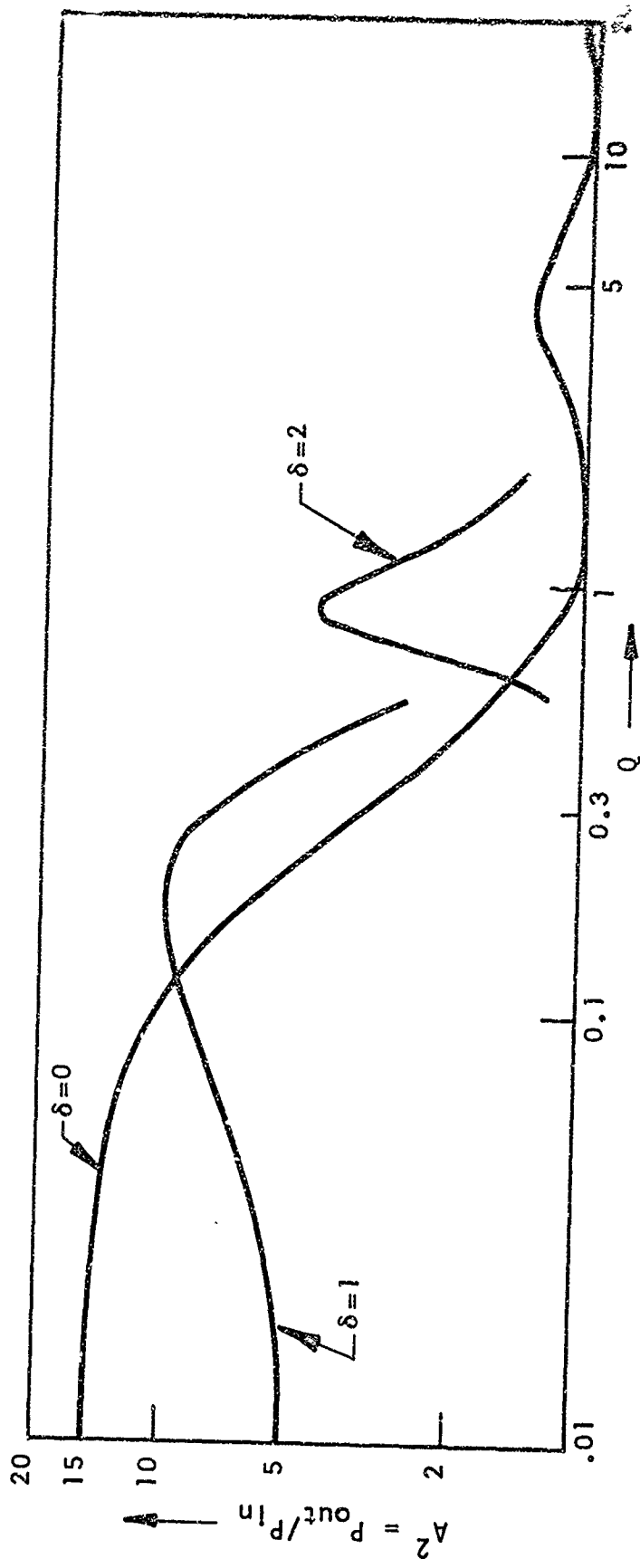
58

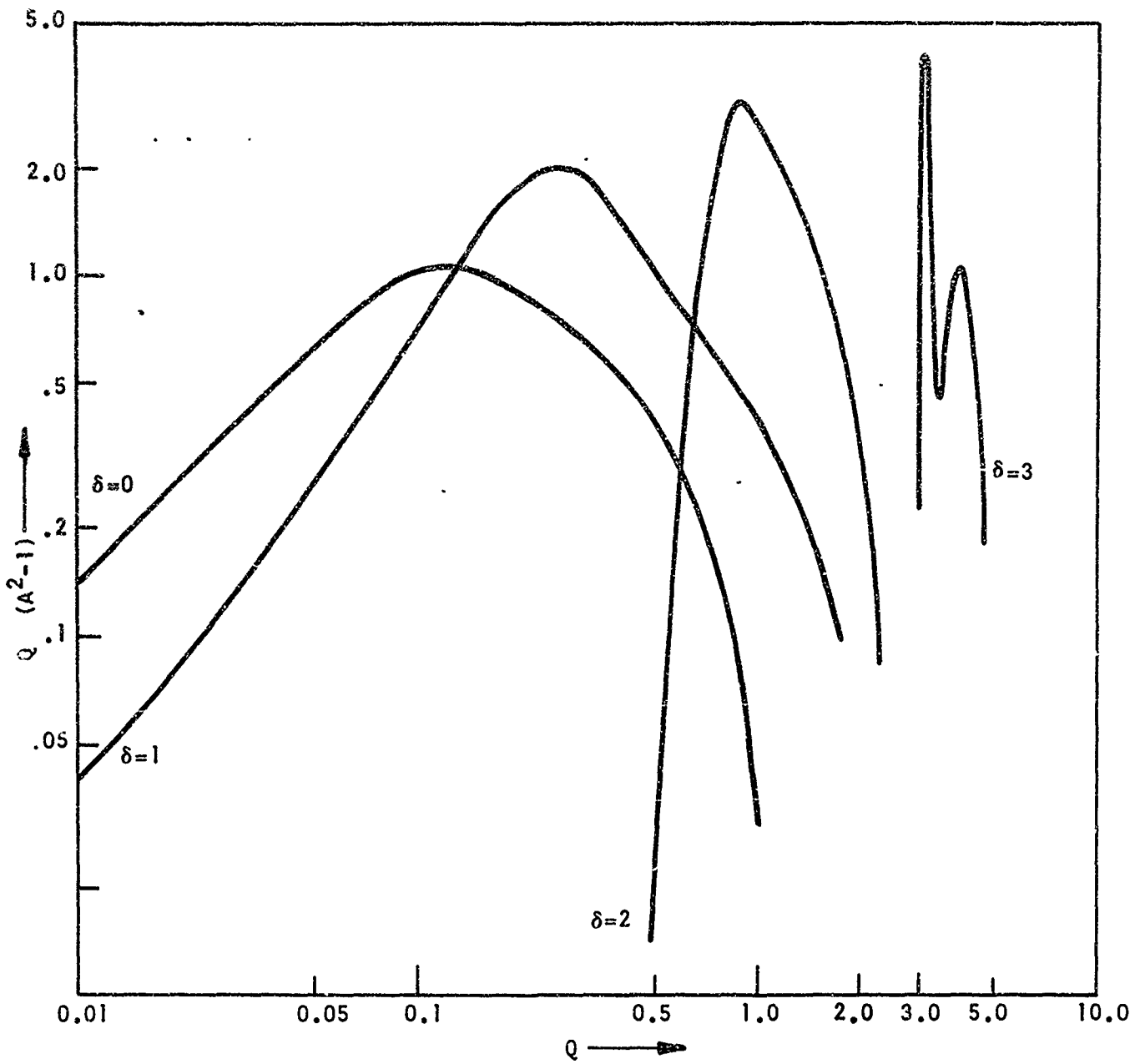FIGURE 9 LARGE-SIGNAL GAIN VS Q (FOR $\alpha_0 \ell = 2.0$)

59

D-9319

FIGURE 10   NORMALIZED EFFICIENCY VS Q (FOR $\alpha_o \ell = 2.0$)

D-9309

60

In Figure 9, we also show curves for $\delta = 2$ and $\delta = 3$. It is perhaps somewhat surprising that the peak electronic efficiency continues to improve with increasing δ, roughly by a factor of $(1 + \delta)$. (c.f. Eq. (3.47)). This result was not predicted by the "large gain" theory in Section 3.3.2, which is not surprising since the assumption $Q \ll 1$ eliminates the interesting regions of Figs. 9 and 10 for the $\delta = 2$ and 3 cases.

We verified that the peak value of Q ($A^2 - 1$) does continue to increase with increasing δ for $3 < \delta < 6$. The critical value of Q (for peak P_{el}) scales roughly as $\frac{4}{27} \delta^3$ for large δ; this scaling can be predicted by rough arguments on the necessary shape of $G(\Psi)$ in Fig. 7 for the case $Q \gg 1$, $\delta \gg 1$. The gain at peak P_{el} is therefore very small for large δ, since $(A^2 - 1) \simeq 7/\delta^2$ for $\delta \gg 1$.

Because of the low gain, the improvements in electronic efficiency for $\delta \gg 1$ are of limited practical significance. It is important to stress, however, that the "limit" implied by Eq. (3.52) is not fundamental, and can be improved on somewhat by tolerating a somewhat lower saturated gain.

A set of numerical results for a lower gain amplifier ($\nu_o \ell = 1.5$) are shown in Figs. 11 and 12. In this case, one can go to even higher values of δ (overvoltage even further) before the gain is degraded substantially from the small-signal gain.

3.5 CONCLUSIONS

Most significant results of numerical computations are presented in Figs. 9 + 12. These results show saturations characteristics of synchronous-wave amplifiers due to beam de-synchronization and effects of over-voltaging the beam. Surprising results of these calculations are the saturation characteristics of grossly over-voltaged beams. The
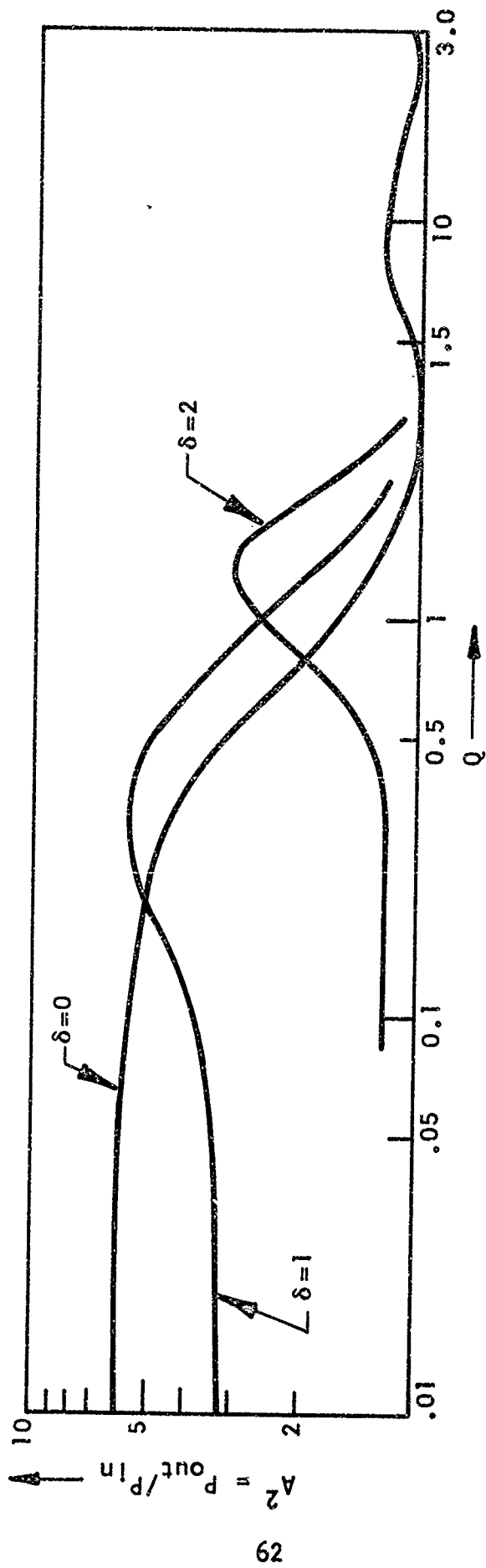
61

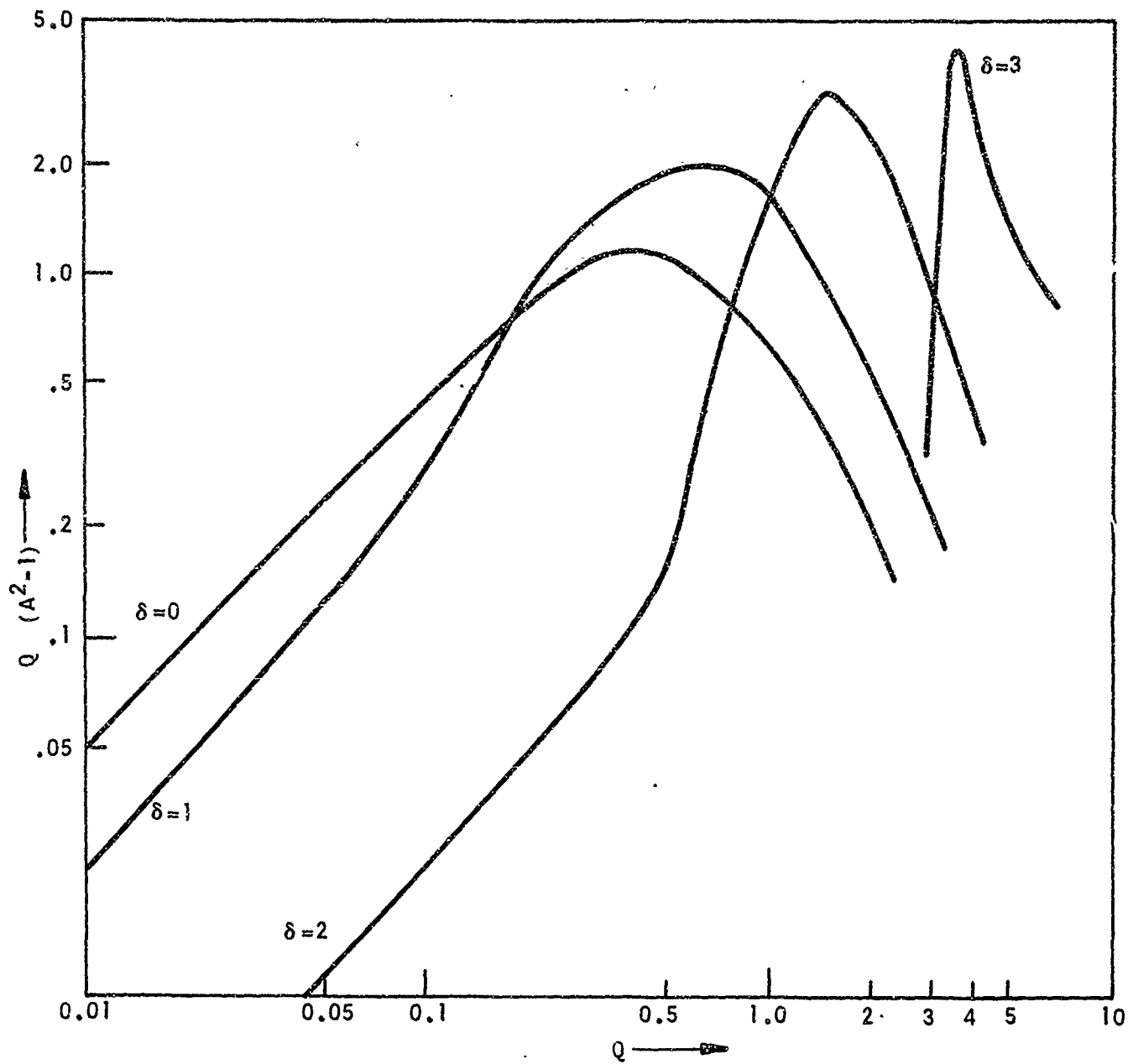FIGURE 11 LARGE-SIGNAL GAIN VS Q (FOR $\alpha_o \ell = 1.5$)

62

29

D-9318

FIGURE 12   NORMALIZED EFFICIENCY VS. Q
(FOR $\alpha_0 \ell = 1.5$)

D-9308

calculated results indicate that the saturation effect due to over-driving can be compensated for by increasing the beam voltage. At input levels approaching a significant fraction of the beam power, one continues to get a small but finite gain. Experimental results (presented in the next section) confirmed these general features of the saturation characteristics of synchronous-wave amplifiers.

These calculated results imply that the efficiency of the transverse-wave interactions (i.e., electronic efficiency) could be raised considerably by proper adjustments of the voltage profile along the length of the interaction space. The voltage could be increased in small steps at appropriate positions (ζ_s) along the tube to increase the saturation level. This process could be continued at least until δ reaches 6. The power saturation limitation specified by Eq. (2.62); therefore, can be overcome relatively easily by shaping of the voltage profile, either tapering or jumping. Nonlinear equations presented in this section provide the prescription for the required voltage shaping for maximum efficiency.

64

IV. EXPERIMENTAL STUDIES

4.1   Introduction

The summary of design equations presented in Section 2.4 pointed out theoretical limitations of the synchronous-wave devices. These computed results indicate that the attainment of a high-efficiency, high-power device is possible if one can find a suitable circuit with a large transverse interaction impedance. Since we were unable to find a suitable transverse-wave circuit with a large interaction impedance, the attainment of a high-efficiency, high-power device was theoretically precluded. For this reason, our experimental study was designed as a diagnostic study to verify the validity of various theoretical predictions so that the design equations presented earlier in Section 2 may be used reliably to project capabilities of transverse-wave amplifiers.

The experimental vehicle designed as a diagnostic tool is described in Section 4.2. The circuit used in the experimental tube was a twisted two-wire line which offers the versatility of being useful for both cyclotron and synchronous-wave interactions. The transverse interaction impedance of the circuit , however, was estimated to be only about 4 ohms. Synchronous-wave experiments are described in Section 4.3. The power saturation characteristics and the velocity spread induced by the RF interaction were measured and related to the theory. Cyclotron-wave interactions were also observed, and results of these experiments are described in Section 4.4.

4.2   Experimental Vehicle

The slow-wave circuit for the study vehicle is a twisted two-wire transmission line. It may also be described as a bifilar helix in which both the longitudinal (even) and the transverse (odd) modes may be excited. The longitudinal mode, however, may be effectively suppressed by a selective

65

excitation, and, because of the wide disparity in the phase velocities of the two modes, the electron beam interaction with the longitudinal mode may be ignored. Johnson[11] has demonstrated that a bifilar helix is an effective and versatile tool for studying transverse-wave interactions.

The dispersion relation for the transverse-mode of the bifilar helix (or, a twisted two-wire line) is approximately

$$\beta = \frac{2\pi}{p} \pm \frac{\omega}{c} \tag{4.1}$$

where p is the pitch of the helix. The expression for the transverse interaction impedance, derived in Appendix B, is

$$K_t = \left[4\beta^2 \; \pi \sqrt{\frac{\epsilon_o}{\mu_c}} \; d^2 \ell n(d/\rho) \right]^{-1} \tag{4.2}$$

where d is the distance between the two wires and ρ is the radius of wires.

Table III contains a list of design parameters for the helix and properties of the circuit calculated from the above equations. The choice of design parameters were dictated by practical considerations of beam size, beam displacement, mechanical design of helix support and available material, as well as the interaction impedance itself. The instantaneous bandwidth of the circuit is quite limited, but frequencies for both the synchronous and cyclotron interactions could be voltage-tuned over a wide range of frequencies.

TABLE III

Design Parameters

Circuit	Bifilar helix (twisted two-wire line)
	I.D. $= .150"$ $f = 0.5 - 1.0$ GHz pitch $= .500"$ $v_p \approx 6 \times 10^8 - 1.2 \times 10^9$ cm/sec wire size $= .030"$ $\beta \approx 5.1/$cm length $= 16"$ $K_t \approx 4.0\ \Omega$
Beam	$V_o = 100 - 500$ volts $I_o = 1 \sim 10$ mA (grid-controlled) Beam diameter $= 0.040"$ Focusing field $\approx 200 - 1000$ Gauss (variable)

The electron gun was designed to operate at beam voltages of 200-1500 volts with beam currents of 1-10mA. To provide the flexibility of varying beam currents, a gridded gun design was chosen. The choice of beam voltage was determined by the synchronism condition with the circuit in the frequency range of 0.3 to 1.0 GHz. The beam current was limited by the (1) current density limitation, (2) considerations of energy spread due to finite beam size discussed in Section 2, and (3) the focusing field requirement. The minimum focusing field required for this beam is approximately 400 gauss. The gun design parameters are also presented in Table III.

Figure 13 shows a sketch of the experimental tube and Fig. 14 is the photograph of the completed tube. The helix is supported by four dielectric rods in a shell of .600" I.D. as shown in Fig. 15.
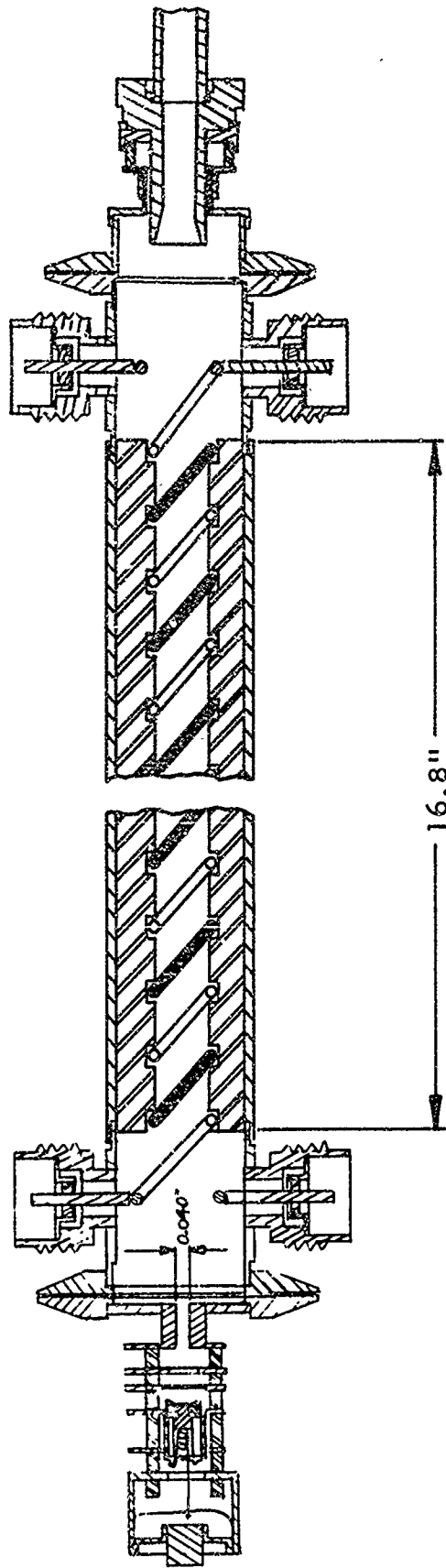
67

FIGURE 13 SKETCH OF THE EXPERIMENTAL TRANSVERSE-WAVE AMPLIFIER

16.8"

0.040"

68

D-8531

FIGURE 14   PHOTOGRAPH OF THE EXPERIMENTAL TUBE

69

D-9307
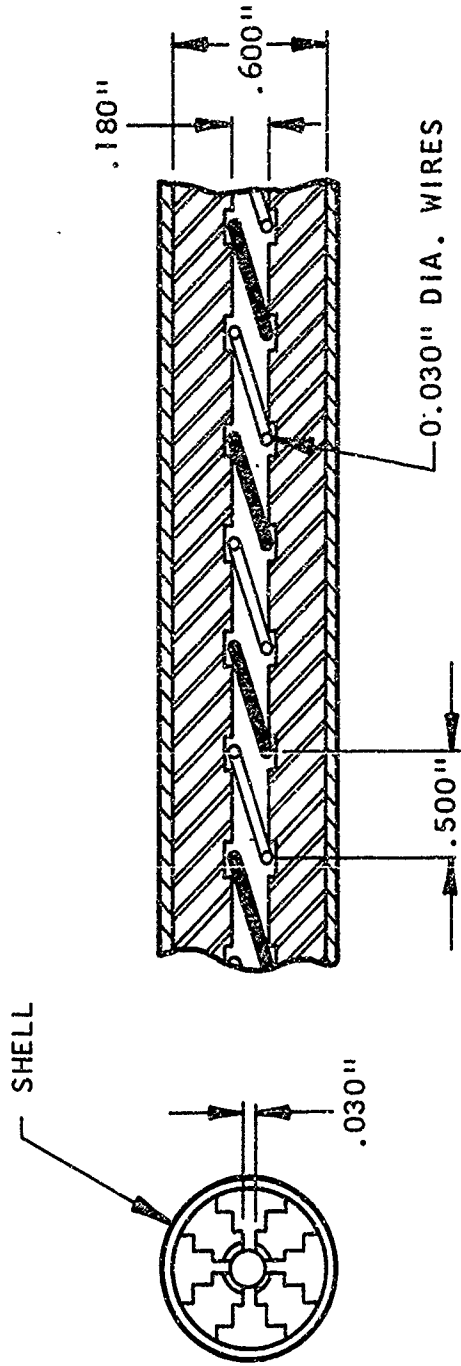
FIGURE 15 DIELECTRIC SUPPORTS FOR BIFILAR HELIX

.180"

.600"

0.030" DIA. WIRES

.500"

SHELL

.030"

70

D-8527

4.3   Synchronous-Wave Interactions

Figure 16 shows the experimental setup. The most effective method of exciting the transverse-wave mode in the "bifilar helix" is to excite two helices 180° out of phase from each other using some sort of balun arrangement. We discovered, however, that highly phase-sensitive setup is undesirable because a small unbalance in the phase caused by the beam could be interpreted erroneously as a large gain. By exciting one helix with the other one shorted to the ground, we were able to obtain a reasonably good coupling to the transverse wave with a transmission loss of approximately 3.5 dB. In the output circuit, the signal from the two helices were added via appropriate phase shifters and a hybrid to insure that all available power is correctly measured.

4.3.1   Gain and Saturation Characteristics

The gain measurements were made by observing the signal output as a function of the beam voltage with the beam current fixed. Figure 17 shows a typical result obtained at 700 MHz. This figure shows that there are at least three distinct modes of interactions between the helix and the beam. To identify the transverse-wave mode, we reversed the direction of the magnetic field. Comparing the two traces in Fig. 17, we see that there are two modes of interactions (one at far right and one at far left) that remain insensitive to the direction of the magnetic field. These two interactions are the space-charge wave interactions; one occurring at low voltage being the Kompfner dip and the one at higher end, the ordinary traveling-wave tube gain. The interaction at 250 volts, which changes its sign with the reversed magnetic field is positively identified as the synchronous gain and dip (depending on the sign of the synchronous wave). Figure 18 shows the ω-β relation required for various synchronous-wave interactions. Another test to
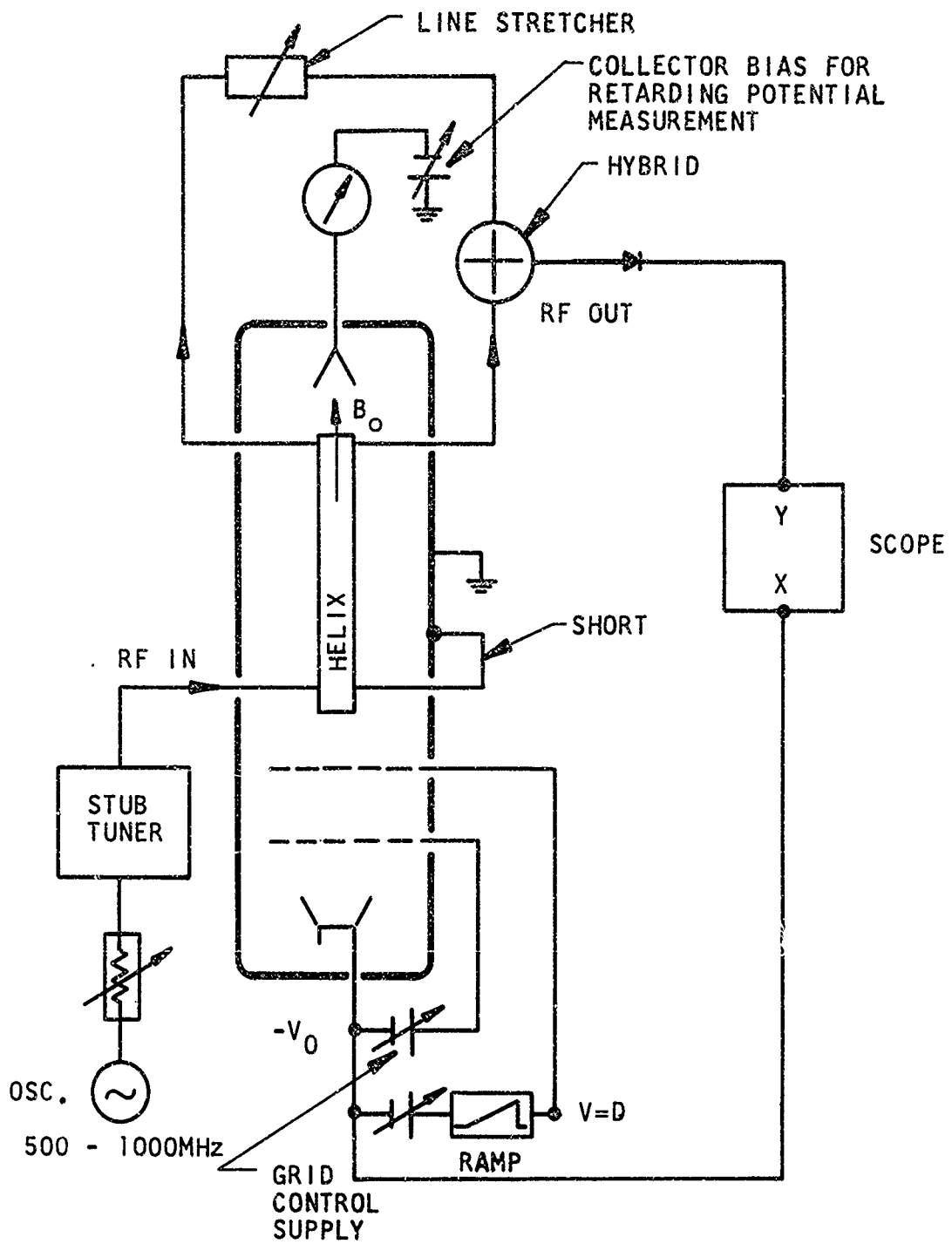
71

FIGURE 16   EXPERIMENTAL SETUP FOR GAIN MEASUREMENT
             AND RETARDING POTENTIAL MEASURMENT
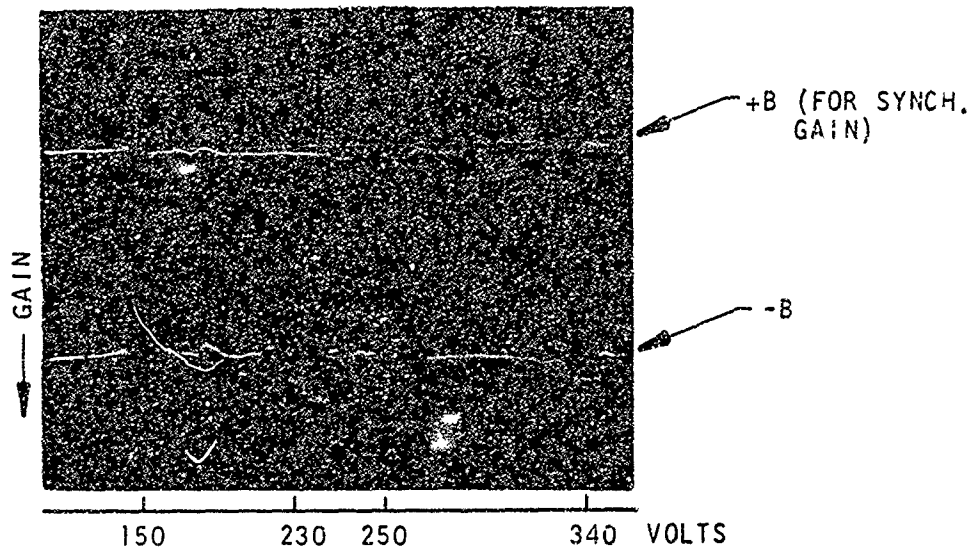
D-8842

72

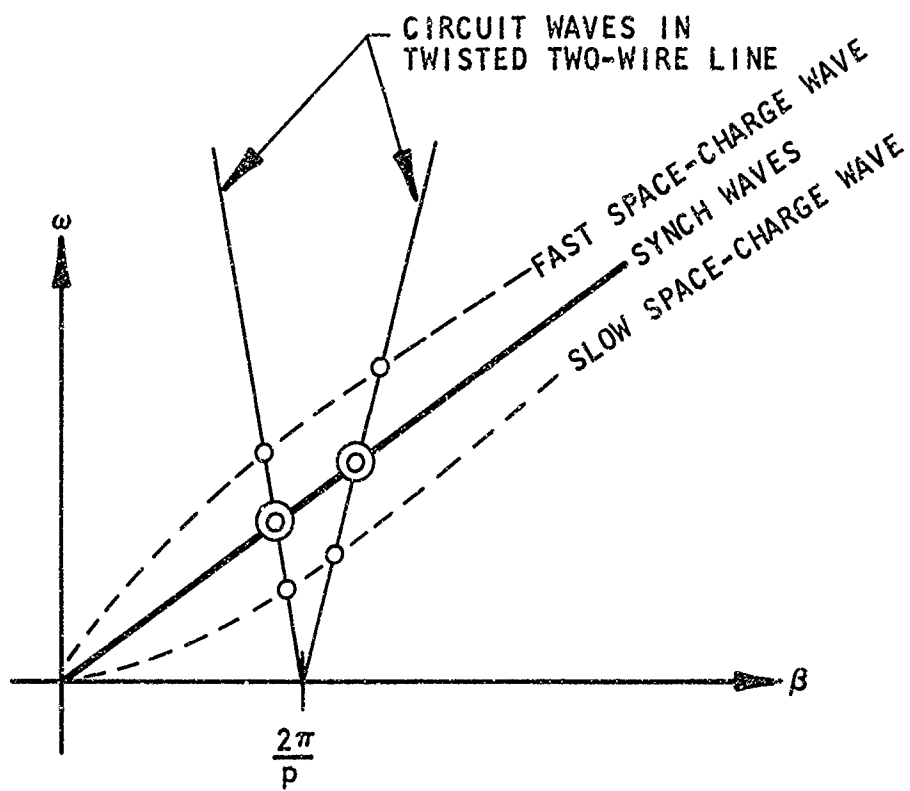FIGURE 17   OUTPUT VS BEAM VOLTAGE (f = 700 MHz, I_o = 5 mA)

73

FIGURE 18 $\omega - \beta$ DIAGRAM SHOWING ALL POSSIBLE INTERACTIONS
INVOLVING SYNCHRONOUS WAVES AND LONGITUDINAL
SPACE-CHARGE WAVES

D-9317

74

identify various modes of interactions is to gradually increase (or decrease) the beam current. With an increase in the current density, the voltages for the longitudinal wave interactions spread apart as expected (since the plasma frequency increases), but the synchronous voltage for the transverse-wave remains insensitive to the magnitude of the beam current. Figure 19 shows a plot of the frequency versus voltage for the synchronous-wave interactions. The theoretical curve for $\omega - \beta v_o$ is super-imposed. Considering the finite size of the beam and the space charges, the observed frequencies are the indication of the synchronous-wave interactions.

The saturation characteristics were measured, again, at 700 MHz. Figure 20 shows the results of our measurements. The small-signal gain calculated from Eq. (2.23) for this tube is roughly 3.0 dB and the corresponding $\alpha_o \ell$ is approximately 0.8. To compare this data with the theoretical saturation characteristic, theoretical curve for $\alpha_o \ell = 0.8$ calculated using formulas developed in Section 3 is also presented in Fig. 20 . Because of the small error in the estimated small-signal gain, the theoretical curve appears to be shifted verically. Except for this discrepancy, the saturation level predicted from the theory is very close to the measured value. The measured curve also shows the same qualitative results noted in Figs. 9 and 11. The saturation characteristics given in Fig. 20 shows that one continues to get finite gain, even when the input drive approaches the beam power level. With 1 watt drive, we obtained as much as 300 mW net gain from the tube with the beam power of 1.5 watts. This corresponds to 20% electronic efficiency.

The over-voltaged behavior of the tube at high input drive is illustrated in Fig. 21. As expected from the results of calculations in Section 3, the beam voltage for maximum gain shifted upward as the input drive was increased. To compare this result with theoretical predictions,

75
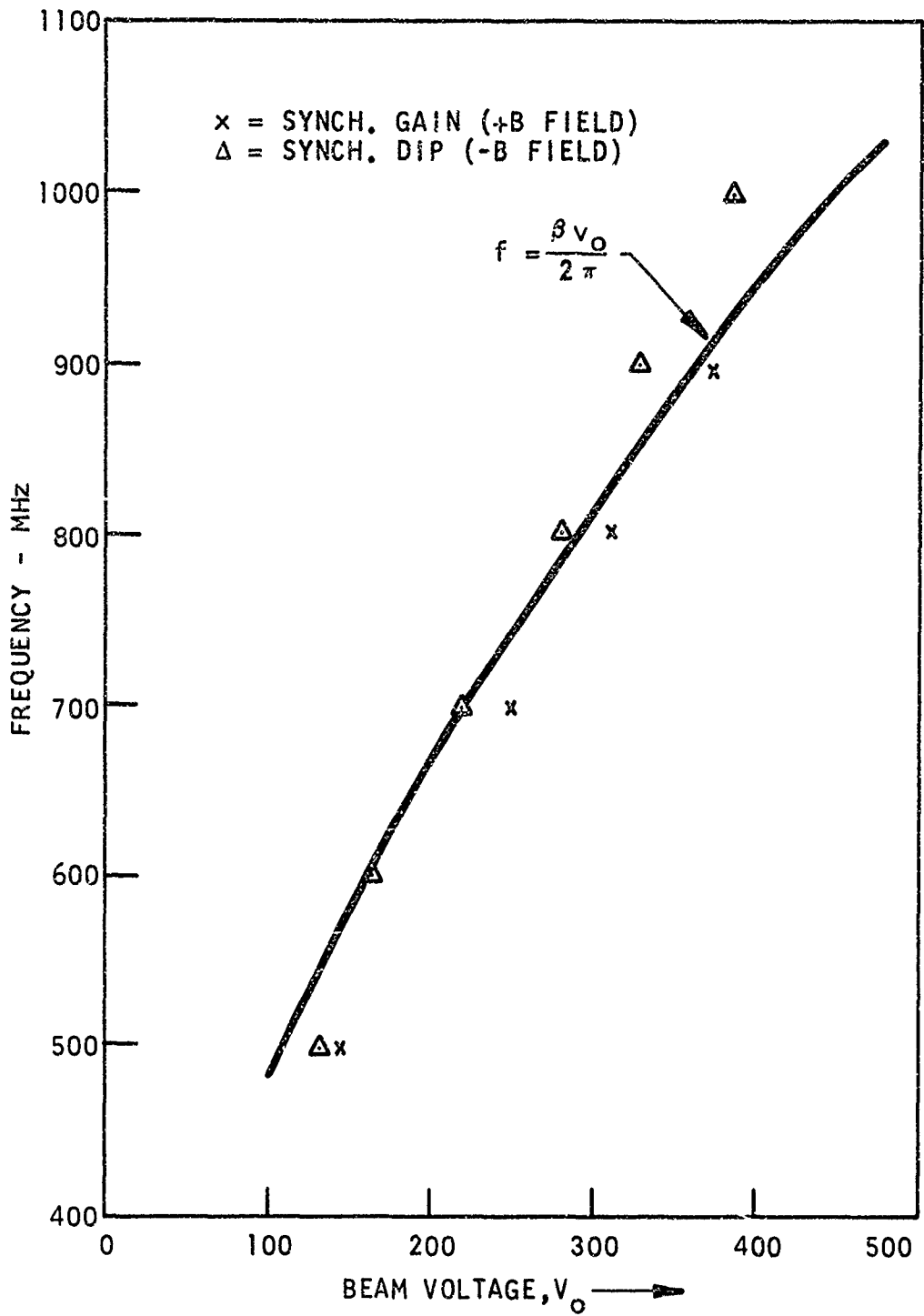
FIGURE 19   FREQUENCY VS BEAM VOLTAGE FOR SYNCHRONOUS-
WAVE INTERACTIONS

D-8844

76
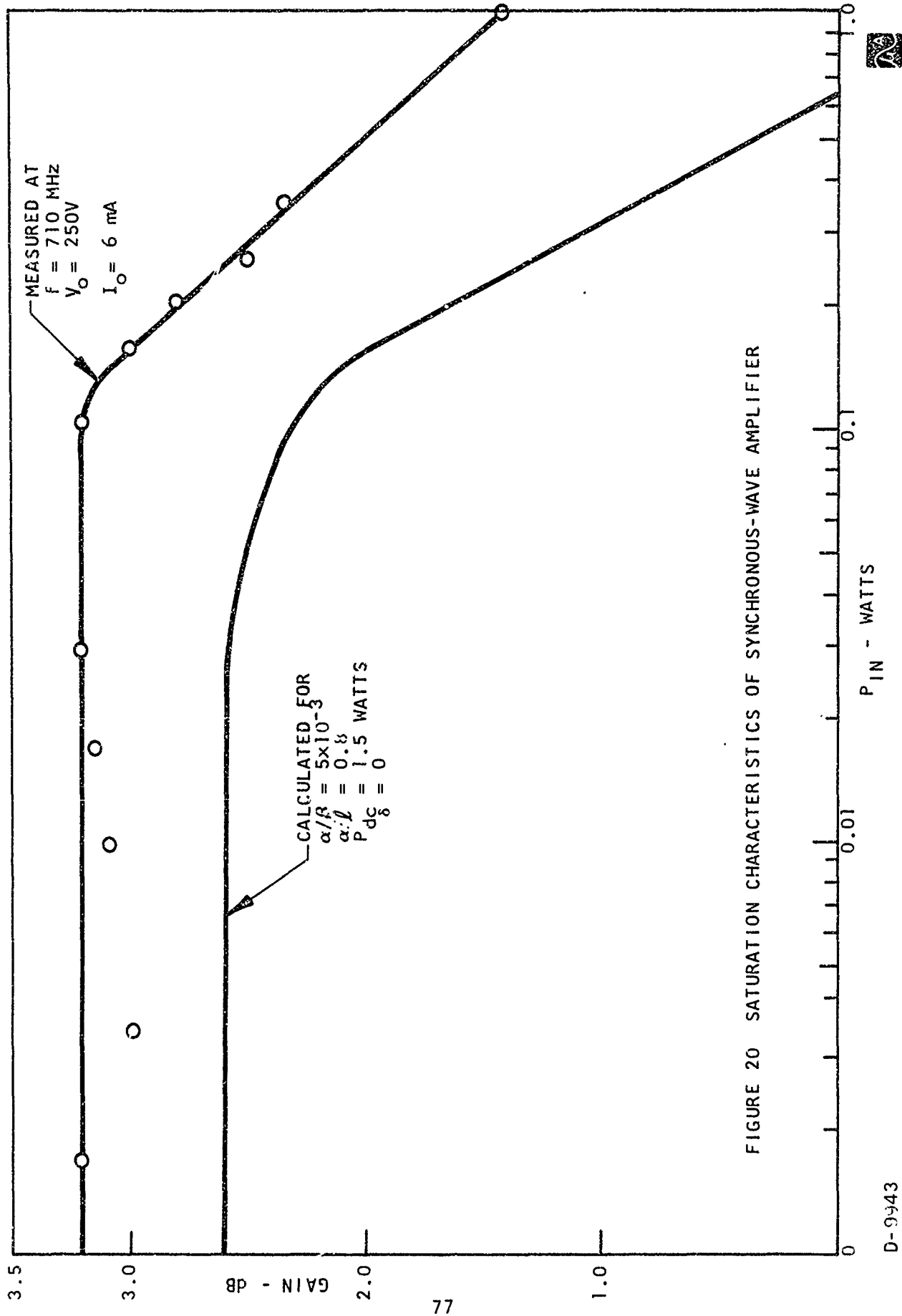
FIGURE 20   SATURATION CHARACTERISTICS OF SYNCHRONOUS-WAVE AMPLIFIER

MEASURED AT
f = 710 MHz
V_o = 250V
I_o = 6 mA

CALCULATED FOR
α/β = 5×10^{-3}
$\alpha \cdot \ell$ = 0.8
P_{dc} = 1.5 WATTS
δ = 0

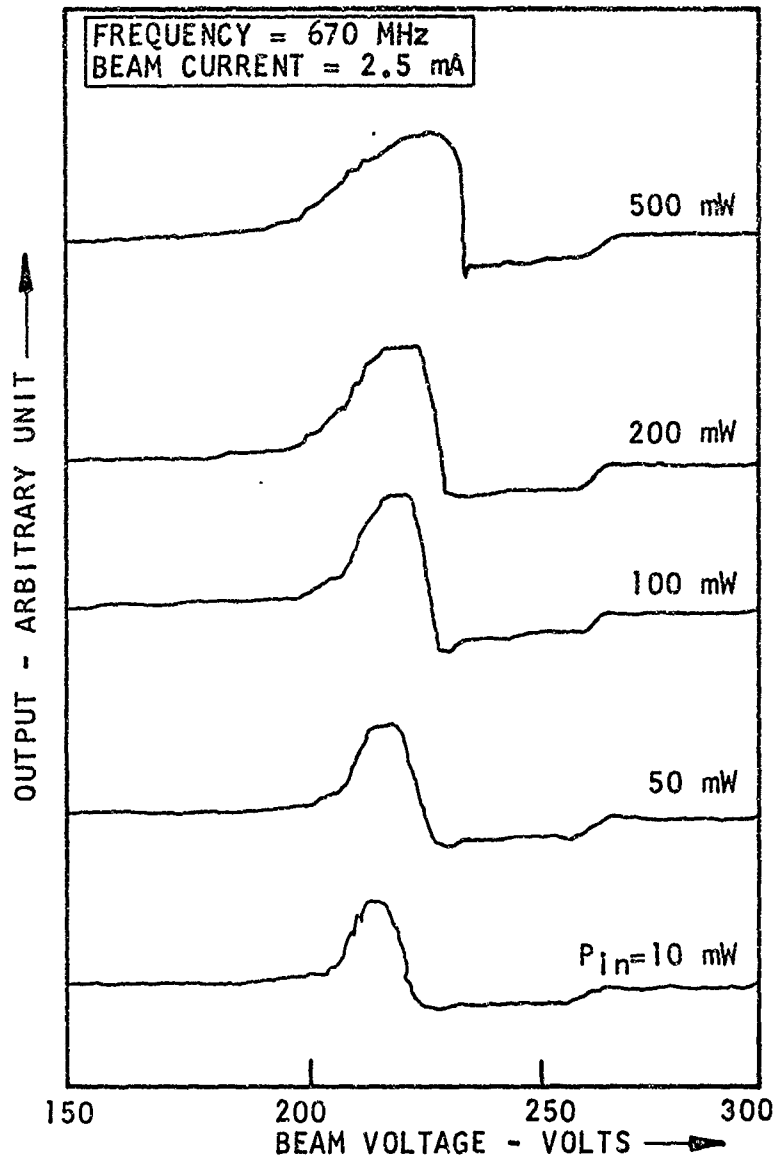P_{IN} - WATTS

GAIN - dB

77

D-9943

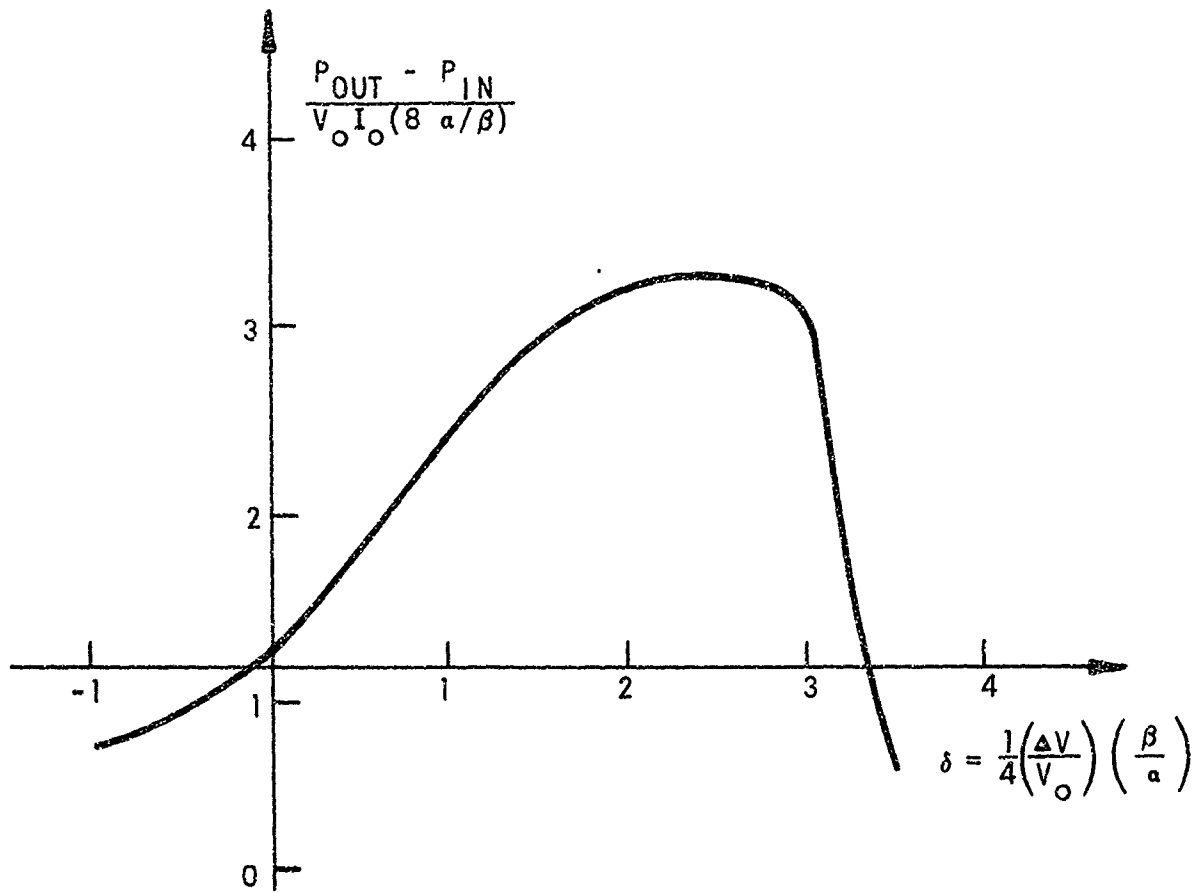FIGURE 21   OUTPUT VS BEAM VOLTAGE SHOWING OVER-DRIVE
CHARACTERISTICS

D-9314

78

we present in Fig. 22, a plot of the power gain as a function of δ. In Fig. 22, δ = 1 corresponds to approximately 3 volts. The calculated form of the velocity dependence of the gain is remarkably similar to measured curves.

4.3.2   Velocity Spread Measurements

The main purpose of the experimental study was to measure the actual velocity spread induced in the beam by the synchronous-wave interaction. To measure the velocity distribution of the "spent" beam, we performed retarding potential measurements on the collector.[19] For this measurement, the collector was negatively biased (relative to the helix), and the collector current was measured as a function of the collector bias. A set of data obtained at 700 MHz with a beam current of 1 mA is shown in Fig. 23. With no input drive, we note that the collector current was space-charge limited when the collector voltage was about 35 volts above the cathode potential, and, therefore, the velocity distribution in the absence of the RF drive could not be measured accurately by this technique. With a strong RF drive, however, there is a marked velocity spread. Since the number of electrons that have lost a substantial portion of their energy is small, the space-charge limitation should not affect the measurement of the <u>lower edge</u> of the electron energy distribution. Results of the retarding potential measurements are useful, therefore, in determining the lowest energy of electrons in the spent beam. Referring to Fig. 4, the energy spread induced by the RF interactions may be calculated as follows

$$\Delta\epsilon_s = (v_o - \Delta\epsilon_L) - V_{min} \qquad (4.3)$$

$$\Delta\epsilon_L = \frac{P_{out} - P_{in}}{I_o} \qquad (4.3a)$$

79

The vertical axis is labeled $\dfrac{P_{OUT} - P_{IN}}{V_o I_o (8\,\alpha/\beta)}$ with marks at 0, 1, 2, 3, 4.

The horizontal axis is labeled $\delta = \dfrac{1}{4}\left(\dfrac{\Delta V}{V_o}\right)\left(\dfrac{\beta}{\alpha}\right)$ with marks at -1, 1, 2, 3, 4.

$$\alpha/\beta = 5\times10^{-3}$$
$$\alpha\ell = 0.8$$
$$Q = P_{IN}/\left[8(\alpha/\beta)\,V_o I_o\right] = 5$$

FIGURE 22 OVER-VOLTAGING CHARACTERISTICS (CALCULATED FOR
$Q = 5$, $\alpha/\beta = 5\times10^{-3}$, $\alpha\ell = 0.8$)

D-8841
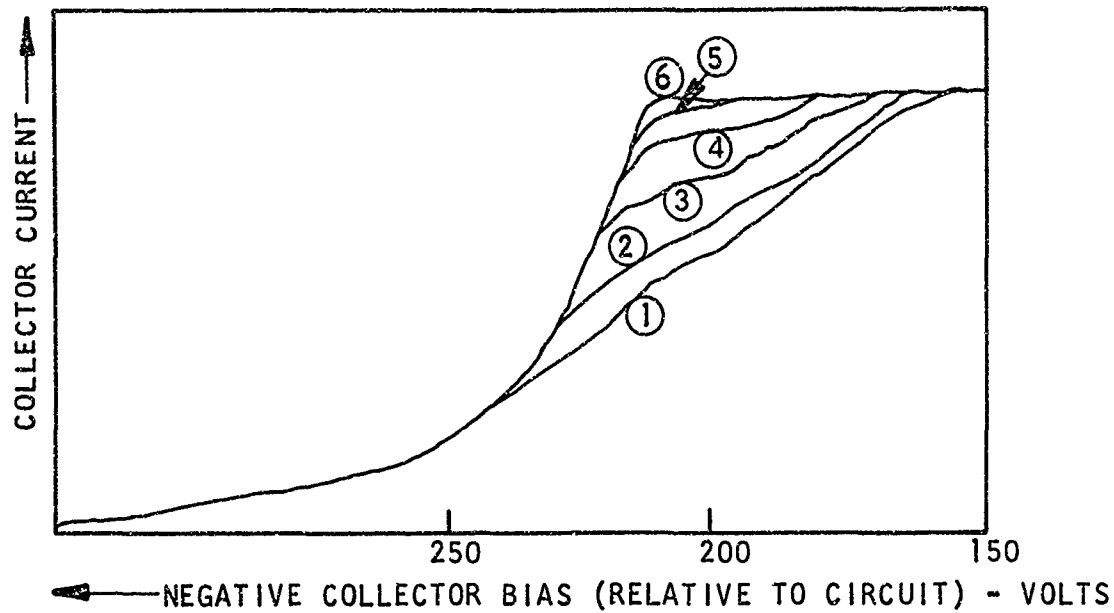
CURVE	P_{in} (mW)	P_{out} (mW)	P (mW)
1	280	310	30
2	145	165	20
3	78	87	9
4	41	47	6
5	21	23	2
6	0	0	0
	I_o=1 mA B_o=800 GAUSS		
	V_o=250 V		
	F=710 MHz		

FIGURE 23   COLLECTOR CURRENT VS RETARDING
POTENTIAL

D-9311

81

where V_o is the initial beam velocity and V_{min} is determined from the measured data (Fig. 23).

According to the theoretical result derived in Section 2, the energy spread may be calculated independently from the net power gained by the circuit wave. From Eqs. (2.53) and (2.54), we get

$$|r_1| = \left[\frac{2(P_{out} - P_{in})}{\omega I_o B_o}\right]^{1/2} \tag{4.4}$$

$$\Delta \epsilon_s = \Delta \epsilon_L (2b/|r_1|) \tag{4.5}$$

The energy spreads calculated from Eq. (4.3) and measured V_{min} are compared to $\Delta \epsilon_s$ calculated from the net power gain and Eq. (4.5) in Table IV. These results are in close agreement for large $\Delta \epsilon_L$. For small values of $\Delta \epsilon_L$, V_{min} could not be measured accurately due to space-charge limitations of collector current

TABLE IV

Comparison of Energy Spread Measured and Calculated

Curve	$P_{out} - P_{in}$ (mW)	$\Delta \epsilon_s$ (from Eq. 4.5) (volts)	V_{min} (measured) (volts)	$\Delta \epsilon_s$ (from Eq. 4.3) (volts)
1	30	75	155	70
2	20	64	165	65
3	9	60	170	71
4	6	49	185	59
5	2	20	195	53
I_o = 1 mA, V_o = 250 Volts				

Although the calculations described above do give a qualitative
confirmation of the validity of the theory of energy spread, it is desirable
for us to develop a more accurate measurement technique which is free
from the space-charge limitations. To do this, we have modified the
design of the collector to reduce the space-charge in front of the
collector without losing the effective cross-section of the beam. Fig. 24
shows a new collector design. Electrons are admitted to the collector
through a rectangular slit which performs the function of limiting the
collector current. A rectangular slit is far more preferable to a circular
aperture since this will allow us to sample all electrons that have been
displaced off axis. The electrons admitted into the analyzer is velocity-
sorted by the usual method.

Fig. 25 shows a typical set of results. The beam focusing was
adjusted for maximum transmission through the slit with no drive. When
the RF drive was increased, the beam transmission through the aperture
was reduced due to the transverse displacement of the beam. Results
presented in Fig. 25 are similar to the data presented in Fig. 23, and
only   improvements are noted in the space-charge limitation.
To obtain the energy distribution function itself, we should differentiate
the collector current with respect to the retarding voltage. This is
accomplished by superimposing on the retarding potential a small
1000 cycle modulation, and measuring the amplitude of the 1000 cycle
component in the collector current. Fig. 26 shows a family of distribution
functions. Because of the odd shape of the curve in the absence of the
RF drive, it was difficult to obtain quantitatively accurate data of the
velocity distribution. These results, nevertheless, show gross distortions
of the energy distribution due to RF interactions. These results are not
predicted by the filamentary beam theory.
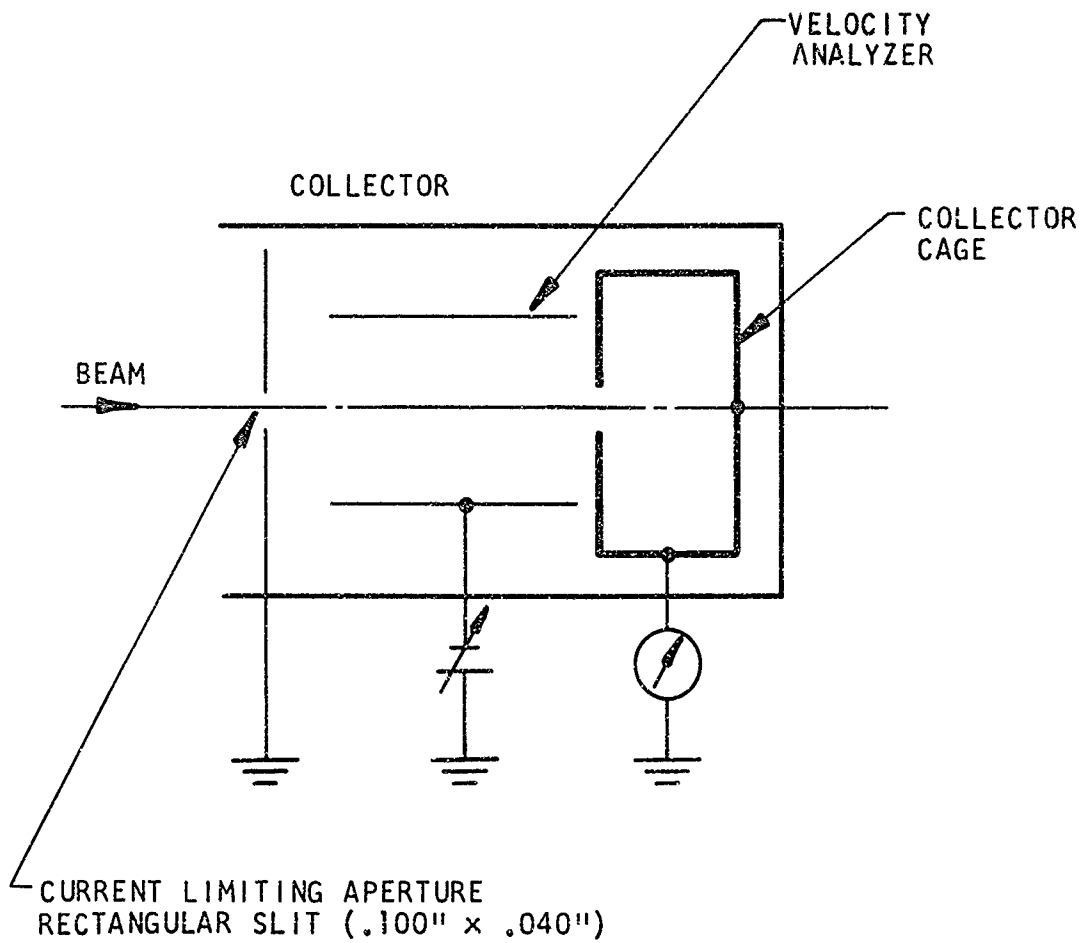
83

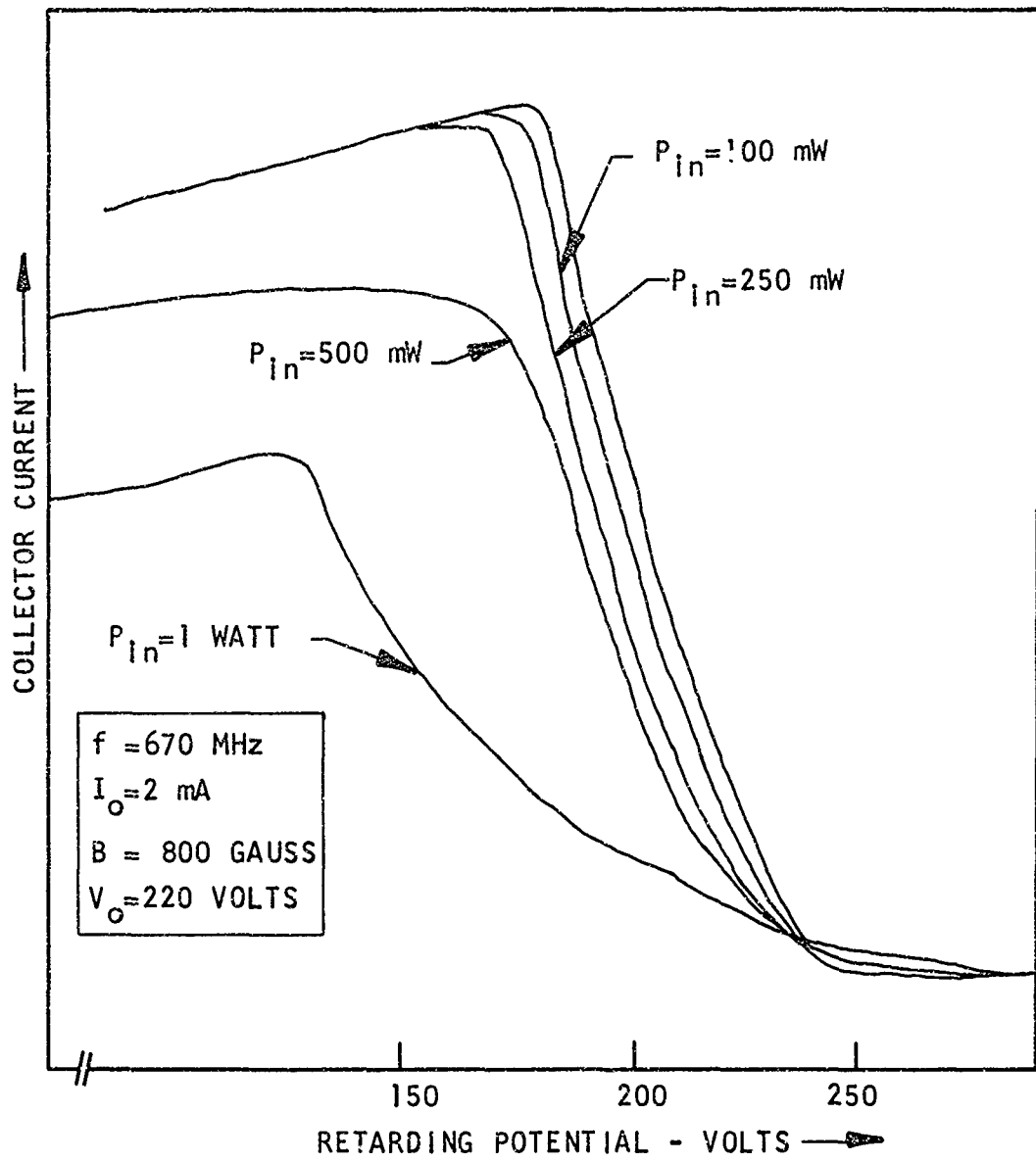FIGURE 24 COLLECTOR WITH VELOCITY ANALYZER

D-8846

FIGURE 25 COLLECTOR CURRENT VS RETARDING POTENTIAL IN
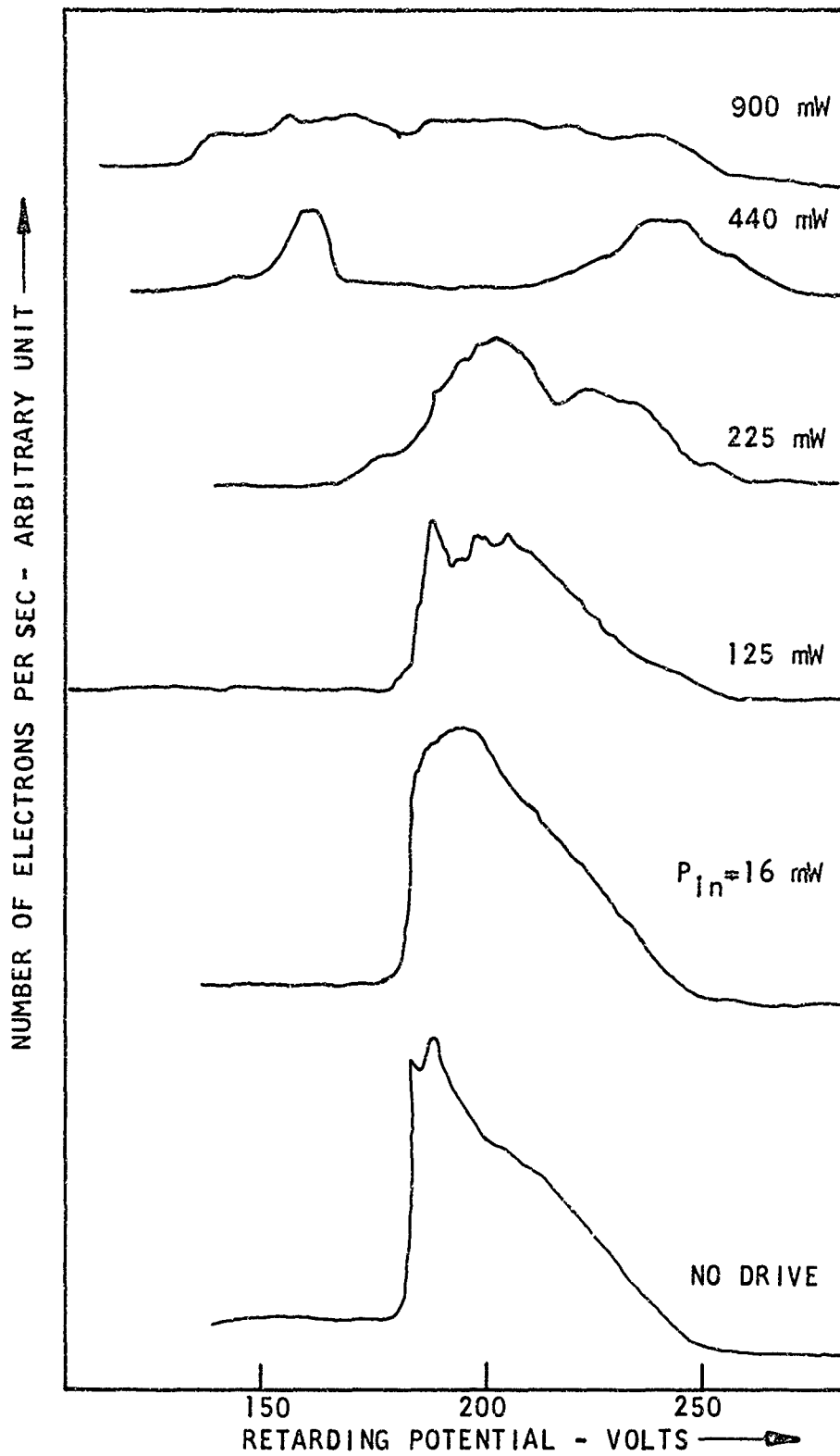THE MODIFIED COLLECTOR

D-9312

FIGURE 26   ELECTRON ENERGY DISTRIBUTION OF SPENT BEAM IN
SYNCHRONOUS-WAVE AMPLIFIER

D-9313

4.4 Cyclotron-Wave Interactions

The synchronou , condition for the interaction between the circuit wave and the slow cyclotron wave is given by (c.f. Fig. 1)

$$\beta = (\omega + \omega_c)/v_o \qquad (4.5)$$

Since β of the circuit is relatively constant ($\beta \simeq 5.1$, c.f. Table III) for all frequencies, this condition could be satisfied by increasing the beam voltage and reducing ω and ω_c. The lowest possible value of ω_c is determined by the beam focusing requirement. In our experiment, the minimum magnetic field required for a reasonable beam transmission was 450 gauss for which $(\omega_c/2\pi) \simeq 1250$ MHz. With the beam voltage of 1200 – 1500 volts, the cyclotron-wave amplification was observed in the frequency range of 350 – 450 MHz. Fig. 27 shows the RF power output vs. voltage. In this type of display, one generally sees interactions of the slow cyclotron wave with both the forward and backward circuit waves. The $\omega - \beta$ diagram for the two interactions is illustrated in Fig. 28. As expected, these interactions occur for the magnetic field directed opposite to the direction for the synchronous-wave amplification. Fig. 29 is a plot of the frequency-voltage relation for the cyclotron-wave (forward-wave) amplification.

The small-signal gain expression for the cyclotron-wave amplification is the same as the one for the synchronous-wave. (Eq. 2.23). Since the beam current is reduced by poor focusing and beam-voltage is increased, the small-signal gain for the cyclotron-wave amplifier is less than in the synchronous-wave device.

According to the theory of energy spread derived in Section 2.3.2, the energy spread induced in the beam by cyclotron-wave interactions is predicted to be much less than in synchronous-wave tubes. As mentioned

87
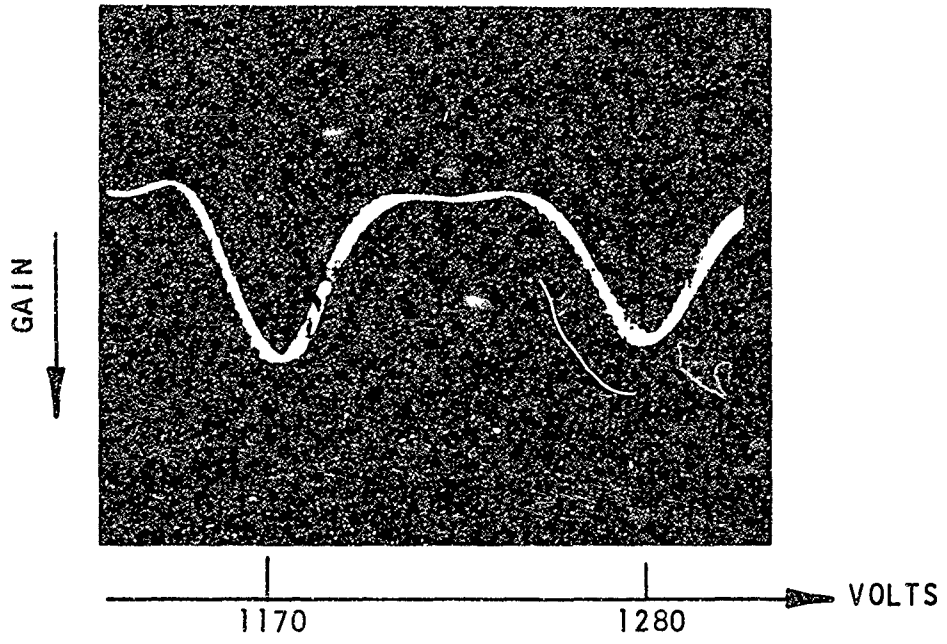
FIGURE 27 OUTPUT VS BEAM VOLTAGE FOR CYCLOTRON-WAVE
(f = 380 MHz, B = 440 G)

D-9306
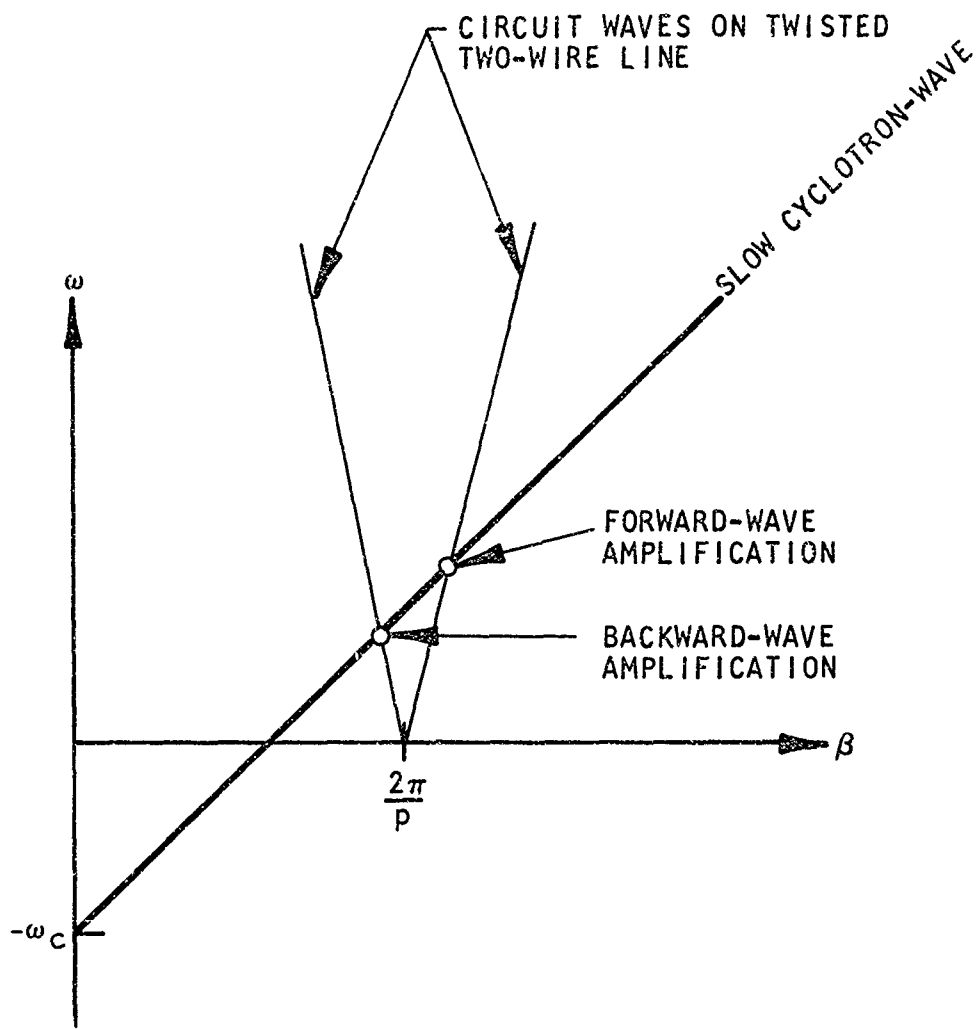
FIGURE 28 ω-β DIAGRAM SHOWING CYCLOTRON-WAVE INTERACTIONS WITH TWISTED TWO-WIRE LINE

D-9316

89
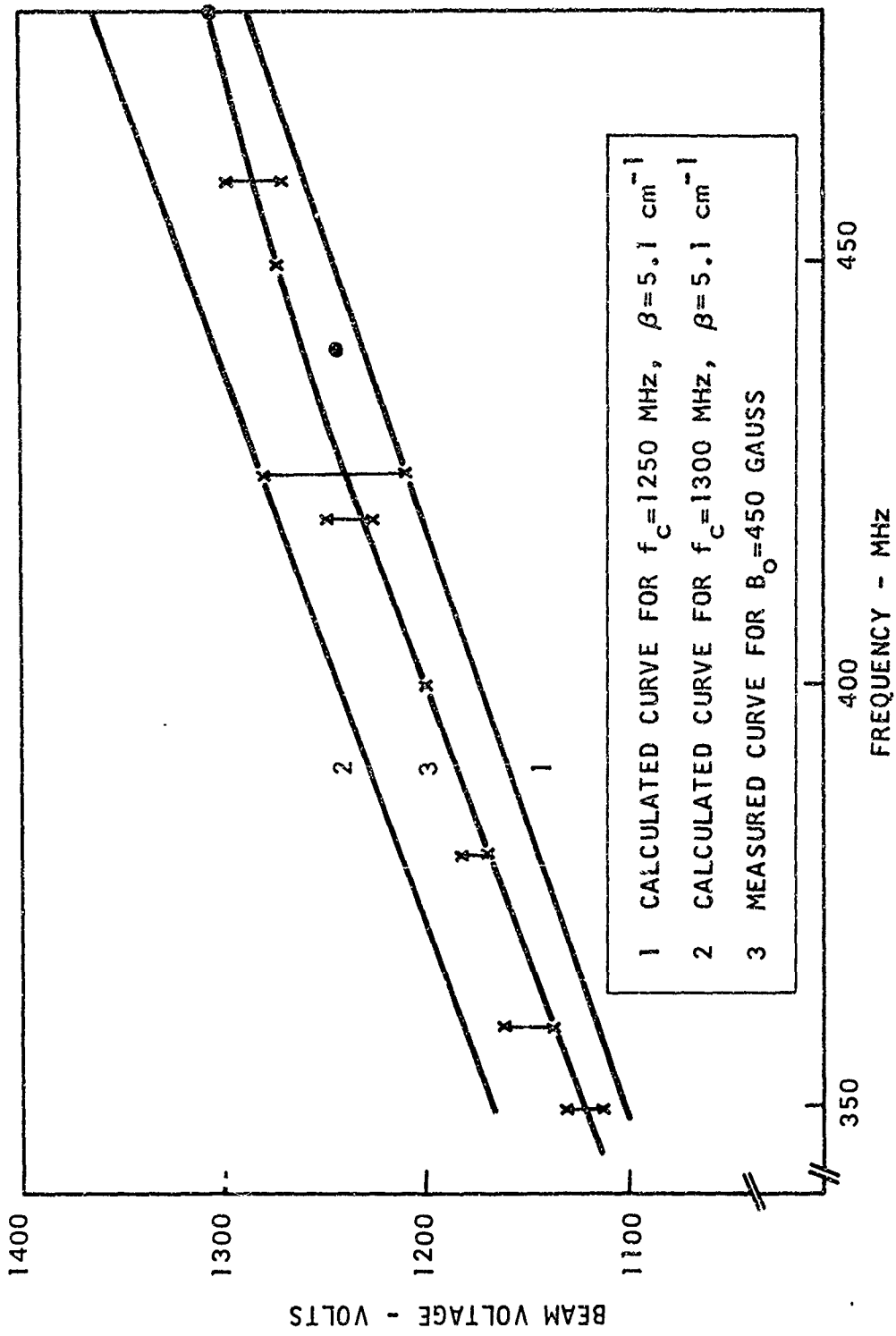
FIGURE 29   FREQUENCY VS BEAM VOLTAGE FOR CYCLOTRON-WAVE
AMPLIFICATION

Legend (inside figure):

1   CALCULATED CURVE FOR f_c=1250 MHz, β=5.1 cm^{-1}

2   CALCULATED CURVE FOR f_c=1300 MHz, β=5.1 cm^{-1}

3   MEASURED CURVE FOR B_o=450 GAUSS

Axis labels:
BEAM VOLTAGE - VOLTS
FREQUENCY - MHz

D-9315

earlier, however, a significant portion of the axial energy is converted into transverse kinetic energy in cyclotron-wave amplifiers. To design collectors for high-efficiency cyclotron-wave amplifiers, one must devise a method of collecting electrons with a sizable transverse kinetic energy.

The energy distribution functions of spent electron beams in cyclotron-wave amplifiers were measured by the same technique employed earlier in the synchronous-wave tube. Figure 30 shows a family of distribution curves, but the interpretation of these results is not simple, because the effect of the retarding voltage (applied via a cylindrical electrode) on the transverse kinetic energy is difficult to analyze.

4.5   Conclusions

Experimental results presented in this section may be summarized as follows:

1. Both the synchronous and the cyclotron wave interactions have been positively identified.

2. The small-signal gain and saturation characteristics of the synchronous-wave amplifiers are in good agreement with theoretical predictions based on the nonlinear theory presented in Section 3.

3. The energy distribution function of the spent beam in synchronous-wave amplifiers have been analyzed to show that the energy spread predicted by the theory in Section 2 gives fairly reliable results.

These experimental results indicate that the design equations derived in Section 2 and the nonlinear behavior predicted in Section 3 may be relied upon in projecting capabilities of high-power transverse-wave amplifiers.

91
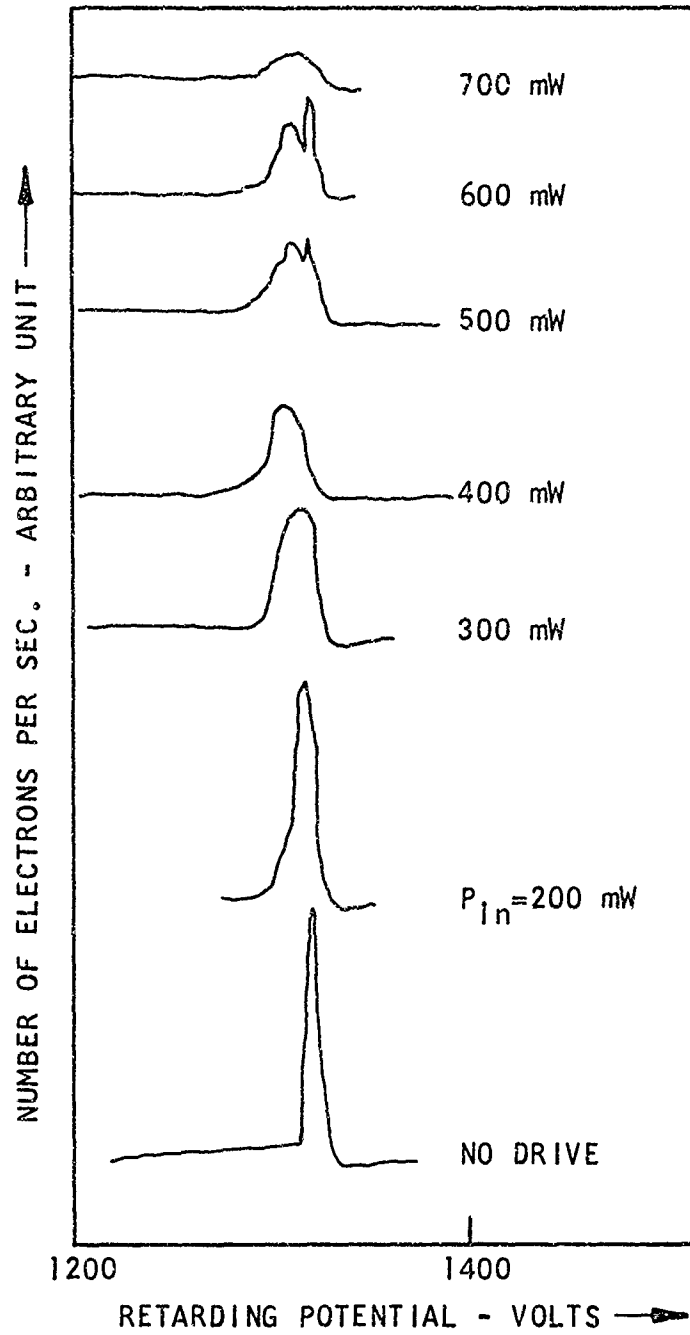
FIGURE 30   ELECTRON ENERGY DISTRIBUTION OF SPENT BEAM IN CYCLOTRON-WAVE AMPLIFIER

D-9310

V. CONCLUSIONS AND RECOMMENDATIONS

We have presented results of a study to evaluate the feasibility of attaining high efficiencies in high-power transverse-wave amplifiers. The analyses presented in Sections 2 and 3 provide the theoretical foundation required to predict the capabilities of high-power transverse-wave tubes that had been unavailable heretofore.

Results of the experimental study presented in Section 4 indicate that our design equations may be used reliably to predict anticipated performance characteristics of synchronous wave amplifiers. Projected capabilities of high-power, high-efficiency, synchronous-wave amplifiers are described in Section 2.4. It was pointed out that efficiencies in excess of 50% are possible with power outputs in kilowatts, provided that a transverse-wave circuit with high transverse interaction impedance (~ 100 ohms) could be found. It was pointed out in Section 3 that the power saturation due to the velocity desynchronization is not a fundamental limitation, and it could be overcome by a simple voltage jumping (or tapering). The nonlinear theory of Section 3 may be used to determine the optimum voltage profile.

A summary of anticipated performance characteristics of high-power transverse-wave tubes is given below.

1. Power Output

A reasonable estimate for the CW power output of transverse wave amplifiers is 2 kW in S-band. This is roughly equal to the best performance of high-power (CW) wideband traveling-wave tubes.

2. Efficiency

Referring to the calculation presented in Table II, we can reasonably expect to operate these high power tubes with efficiencies in the neighborhood of 50%.

93

3. Gain

Because the interaction impedance of the transverse-field circuits is generally low (of the order of 10 ohms), the gain per wave length in transverse wave tubes will be relatively low. For a tube with 10 dB gain in S-band, we would need a tube 18-20 inches long. For tubes longer than 20 inches, we could experience a serious mechanical problem of alignment and construction. The design objective should be set for about 10 dB.

4. Bandwidth

The twisted two-wire line we have been experimenting with has a very limited bandwidth. In fact, most twisted structures that we know of have limited bandwidth, and, therefore, we do not expect the bandwidth of the device to be much greater than about 10%. It should be pointed out, however, the device is voltage tunable over a tremendous frequency range. The tuning range should cover all of L and S bands.

Based on our conclusions, it is apparent that the future effort should be directed toward developing new circuits with high interaction impedance and broader bandwidth capabilities. Since most of the known twisted structures have low transverse interaction impedance, the possibility of selectively exciting a circularly polarized wave in non-twisted structures should be investigated. A reasonable care must be exercised in the selection of the circuit, however, to avoid oscillations (and subsequent beam blow-up) due to the presence of spurious modes.

The analysis in Section 2 showed that the axial velocity spread in cyclotron-wave amplifiers is expected to be much less. It was also pointed, however, that in a cyclotron-wave device, one has to contend with the problem of transverse kinetic energy. This problem has not been considered in detail in this program. A further study of cyclotron-wave amplifiers may be fruitful. Although capabilities of cyclotron-wave

94

devices remain relatively unexplored, we feel that the device capabilities
outlined above represent the most optimistic performance expected in the
immediate future, assuming no dramatic new concept is developed in the
near future.

VI. REFERENCES

1.   A. E. Siegman, "Waves on a filamentary electron beam in
      a transverse-field slow-wave circuit", J. Appl. Phys., vol. 31
      pp. 17-26 January 1960.

2.   R. W. Gould and C. C. Johnson, "Coupled mode theory of
      parametric amplification", J. Appl. Phys., vol. 32, pp. 248-258,
      February 1961.

3.   R. Adler, G. Hrbek and G. Wade, "A low-noise electron-
      beam parametric amplifier", Proc. IRE, vol. 46, pp. 1756-
      1757, October 1958; also Proc. IRE, vol. 47, pp. 1713-
      1723, October 1959.

4.   R. Adler and G. Hrbek, "Nondegenerate electron beam
      parametric amplifier", IEEE Trans., vol. ED-10, pp 1-7,
      January 1963.

5.   A. Bridges, "A low-noise microwave quadrupole amplifier",
      Proc. IRE, vol. 49, pp. 1016-1020, June 1961.

6.   A. E. Siegman, "The d-c pumped quadrupole amplifier -
      A wave analysis", Proc. IRE, vol. 48, pp. 1750-1755,
      October 1960.

7.   J. C. Bass, "Microwave amplification in electrostatic
      ring structures", Proc. IRE, vol. 49, pp. 1424-1425,
      September 1961; "A d-c pumped amplifier with a two-
      dimensional field structure", Proc. IRE, vol. 49, pp. 1957-
      1958, December 1961.

8.   T. Wessel-Berg and K. Blotekjaer, "A d-c pumped amplifier
      using a space-periodic magnetic field", Proc. IRE, vol. 50,
      p. 2513, October 1962.

9.   T. Wessel-Berg, "Electronic interaction theory for transverse-
      wave couplers", J. Elec. Control, vol. 14, pp. 137-166,
      February 1963.

10.   J. E. Carroll, "A transverse-wave traveling-wave tube", Proc.
      5th Int. Microwave Tube Cong., pp. 69-72, Academic Press, Inc.,
      New York, N.Y. 1965.

11. C. C. Johnson, "An investigation of the magnetic transverse waves on an electron beam", IEEE Trans., vol. ED-9, pp. 288-295, May 1962.

12. R. D. Hayes, "A synchronous-wave amplifier", IEEE Trans., vol. ED-11, pp. 98-101, March 1964.

13. C. B. Crumly, "Transverse-Wave High Power Tube, "ECOM-0226-F, Final Report, Contract DAAB07-67-C-0226, Zenith Radio Research Corporation, Menlo Park, Calif., June 1968.

14. W. H. Louisell, Coupled Mode and Parametric Electronics, John Wiley and Sons, Inc., New York, N.Y. 1960.

15. J. E. Carroll, "Effects of space charge on transverse waves in electron beam", J. Elec. Control, vol. 16, pp. 633-651, 1964.

16. T. Wessel-Berg, "A thick-beam analysis for transverse-wave propagation on electron beams", Proc. 4th Micro-wave Tube Cong., pp. 657-662, Centrex Pub. Co., Eindhoven, The Netherlands, 1963.

17. M. Chodorow and C. Sussking, Fundamentals of Micro-wave Electronics, McGraw Hill Book Co., New York, N.Y. 1964.

18. J. E. Rowe, Nonlinear Electron-Wave Interaction Phenomena, Academic Press, Inc., New York, N.Y. 1965.

19. M. Caulton, "Retarding Field Analyzers for the Measurement of Axial Velocity Distributions in Electron Beams," RCA Rev., 26, 217 (1965).

97

Appendix A

Nonlinear Equation for Cyclotron Wave Interaction

In this appendix, we will derive the nonlinear differential equation for the circuit field for the cyclotron-wave interactions. It will be shown that the form of the equation is exactly the same as Eq. (3.17) which was derived specifically for the synchronous-wave interaction.

For the slow cyclotron wave case, we need a right-polarized circuit mode or a reversed magnetic field; for simplicity we choose the latter course and let $\omega_c \rightarrow -\omega_c$ in Eq. (3-3). The beam displacement will now be of the form

$$r(t, z) = R(t, z) e^{-j\omega_c t} \tag{A-1}$$

where R is assumed to be slowly varying on the scale of one cyclotron period. $\left(\dfrac{dR}{dt} \ll \omega_c R \right)$. The transverse equation of motion is approximately

$$\frac{dR}{dt} = \frac{-j\eta}{\omega_c} E_c e^{j\omega_c t} \tag{A-2}$$

Except for this change in the force law, the analysis up to Eq. (3-10) is also applicable to the cyclotron wave case. Energy conservation is now modified as follows. The power per unit length into the electrons is

$$-e\lambda_o \bar{v} \cdot \bar{E} = -|I_o| E_{zb} - \lambda_o e Re (v E_c^*) \tag{A-3}$$

98

Since $v \simeq -j\omega_c r$ for the cyclotron wave,

$$\mathrm{Rev}E_c^* \simeq \mathrm{Re}\,(-j\omega_c r E_c^*)$$

$$\simeq \frac{-\omega_c}{\beta_o}\, E_{zb} \tag{A-4}$$

Therefore

$$\frac{\partial P_c}{\partial z} \simeq |I_o|\, E_{zb}\,\left(1 - \frac{\omega_c}{\beta_o v_o}\right)$$

$$\cong |I_o|\, E_{zb}\left(\frac{1}{1 + \omega_c/\omega}\right) \tag{A-5}$$

$$\beta_o \approx \frac{\omega + \omega_c}{v_o} \tag{A-6}$$

for cyclotron waves. It then follows that the coupling constant is

$$c = \frac{j\beta_o^3 K_t |I_o|}{1 + \omega_c/\omega} \tag{A-7}$$

the differential equation for $\widetilde{E}(z)$ (see Eq. 3.17) how becomes

$$\frac{\partial^2 \widetilde{E}}{\partial z^2} + j\left[\frac{\omega + \omega_c}{v_z} - \beta_o\right]\frac{\partial \widetilde{E}}{\partial z} - \alpha_o^2\,\widetilde{E} = 0 \tag{A-8}$$

where α_o^2 is given by (2.23), with the appropriate β_o (Eq. A-6).

99

The final differential equation for the normalized field is exactly the same as for the synchronous case, (3-26), except that now

$$\delta = \frac{1}{2} \left[\frac{\beta_o - (\omega + \omega_c)/v_o}{\alpha_o} \right] \qquad (A-9)$$

and

$$Q = \frac{\beta_o}{\alpha_o} \frac{(1 + \omega_c/\omega)}{8V_o I_o} P_{in} \qquad (A-10)$$

100

APPENDIX B

Transverse Interaction Impedance of Twisted Two-Wire Line

The interaction impedance may be estimated from the characteristic impedance of the two-wire line, assuming a gentle twist ($p/R \gtrsim 1$). The characteristic impedance of the two-wire line is

$$Z_o = \sqrt{\frac{\mu_o}{\epsilon_o}} \; \frac{\ln(d/\rho)}{\pi} \tag{B.1}$$

where d and ρ are the distance between the two wires and the wire radius respectively. The transverse electric field at the midpoint between the wires is related to the "circuit" voltage by the following expression

$$\left| E_t(o) \right| = \frac{|V|}{d \ln(d/\rho)} \tag{B.2}$$

and the transverse electric field of one circularly polarized component (+1 polarization) in the twisted line is

$$\left| E_{+1}(o) \right| = \frac{1}{2} \left| E_t(o) \right| = \frac{|V|}{2d\ln(d/\rho)} \tag{B.3}$$

The power flow along the circuit may be expressed as

$$P_c = \frac{|V^2|}{2Z_o} = \frac{2d^2\ln^2(d/\rho) \left| E_{+1}(o) \right|^2}{Z_o} \tag{B.4}$$

101

The transverse interaction impedance is, therefore, given by

$$K_t = \left| E_{+1}(o) \right|^2 / 2\beta^2 P_c = \left[4\beta^2 \pi \sqrt{\frac{\epsilon_o}{\mu_o}} \, d^2 \, \ell n(d/\rho) \right]^{-1} \qquad (B.5)$$

102

DOCUMENT CONTROL DATA - R & D		
Security classification of title, body of abstract and indexing annotation must be entered when the overall report is classified)		
1 ORIGINATING ACTIVITY (Corporate author) Microwave Associates, Inc. Burlington, Massachusetts 01803	2a. REPORT SECURITY CLASSIFICATION UNCLASSIFIED	
	2b GROUP	

3 REPORT TITLE

STUDY OF CYCLOTRON & SYNCHRONOUS WAVE DEVICES

4 DESCRIPTIVE NOTES (Type of report and inclusive dates)
Final Report, 1 July 1968 to 30 June 1970

5 AUTHOR(S) (First name, middle initial, last name)

Richard J. Briggs

S. Francis Paik

6 REPORT DATE September 1970	7a. TOTAL NO. OF PAGES 108	7b. NO. OF REFS 19
8a. CONTRACT OR GRANT NO. DAAB07-68-C-0398	9a. ORIGINATOR'S REPORT NUMBER(S)	
b. PROJECT NO		
c.	9b. OTHER REPORT NO(S) (Any other numbers that may be assigned this report) ECOM-0398-F	
d.		

10 DISTRIBUTION STATEMENT

This document has been approved for public release and sale; its distribution is unlimited.

11 SUPPLEMENTARY NOTES	12. SPONSORING MILITARY ACTIVITY U. S. Army Electronics Command Fort Monmouth, New Jersey 07703 AMSEL-KL-TM

13 ABSTRACT

It has been speculated for many years that microwave beam tubes using cyclotron and synchronous wave interactions could have a higher efficiency than is presently attainable in ordinary TWT's. This observation is based on the analysis of filamentary beam model which predicts that all electrons will lose an equal amount of axial energy when they interact with a circularly polarized traveling-wave circuit field. Under ideal conditions, therefore, the collector potential may be depressed close to the cathode potential; thus, very high efficiencies could be realized.

A theory of transverse-wave interactions with a more realistic model of the beam is developed to show that the main practical limitation arises from the fact that a moderate power electron beam must have a non-zero size and non-zero space charge density. The analysis of these effects leads to the following expression for the optimum efficiency with collector depression:

$$\text{Efficiency} \quad 1/[1 + (\text{beam diameter}/\text{r-f beam displacement})]^{-1}$$

A nonlinear theory of the transverse-wave tubes is also developed to predict the saturation output power attainable. Unlike the large-signal theory of TWT's, it is possible to describe the nonlinear behavior of transverse-wave tubes by a simple analytic expression. Numerical calculations of saturation characteristics are presented. The over-voltaged behavior of the tube under strong input drive is calculated to show that the power saturation due to velocity de-synchronization could be overcome by increasing the beam voltage.

DD FORM 1473 REPLACES DD FORM 1473, 1 JAN 64, WHICH IS OBSOLETE FOR ARMY USE.

14 KEY WORDS	LINK A		LINK B		LINK C	
	ROLE	WT	ROLE	WT	ROLE	WT
Transverse Wave Tube						
Traveling Wave Tube						
High Efficiency						
Depressed Collector						
Transverse Wave Interaction						
Synchronous Wave						
Cyclotron Wave						

DOCUMENT CONTROL DATA - R & D

(Security classification of title, body of abstract and indexing annotation must be entered when the overall report is classified)

1 ORIGINATING ACTIVITY (Corporate author)	2a. REPORT SECURITY CLASSIFICATION
	2b. GROUP

3 REPORT TITLE

4 DESCRIPTIVE NOTES *(Type of report and inclusive dates)*

5 AUTHOR(S) *(First name, middle initial, last name)*

6 REPORT DATE	7a. TOTAL NO. OF PAGES	7b. NO. OF REFS

8a. CONTRACT OR GRANT NO	9a. ORIGINATOR'S REPORT NUMBER(S)
b. PROJECT NO	
c.	9b. OTHER REPORT NO(S) *(Any other numbers that may be assigned this report)*
d.	

10 DISTRIBUTION STATEMENT

11 SUPPLEMENTARY NOTES	12 SPONSORING MILITARY ACTIVITY

13 ABSTRACT (continued)

Considering practical limitations of the beam parameters and the saturation characteristics, a set of possible design parameters of a high efficiency (>50%), moderate power level ($\approx$ 1 KW) transverse-wave tube is obtained. The attainment of such goals with a reasonable circuit length appears difficult but is not excluded by our theory.

An experimental low-power vehicle operating in the 500-1000 MHz band was constructed to test the above theoretical predictions. Both the synchronous and the cyclotron wave interactions have been observed. The small-signal behavior as well as the saturation characteristics were in good agreement with the theory. Retarding potential measurements were made to determine the energy spread induced by the RF interactions. Experimental results, in general, tend to confirm the validity of the theoretical results.

DD FORM 1473 REPLACES DD FORM 1473, 1 JAN 64, WHICH IS OBSOLETE FOR ARMY USE.